Pharmacogn. Res., 2026; 18(2):568-584.
https://www.phcogres.com

Original Article

Formulation of a Bioactive Nanoemulsion of Gamma Linolenic Acid for Anti-Glioblastoma Activity

Renu Chaudhari[1,2,*], Farhan Jalees Ahmad[1], Khalid Khan[2], Sayeed Ahmad[3]

[1]Department of Pharmaceutics, School of Pharmaceutical Education and Research, Jamia Hamdard, New Delhi, INDIA.
[2]Department of Regulatory Affairs, Fermish Clinical Technologies Pvt. Ltd., Noida, Uttar Pradesh, INDIA.
[3]Bioactive Natural Product Laboratory, School of Pharmaceutical Education and Research Jamia Hamdard, New Delhi, INDIA.

ABSTRACT

Background: Glioblastoma (GBM), a highly aggressive primary brain tumor, presents significant therapeutic challenges due to its inherent chemoresistance, neurotoxicity concerns, and the formidable blood-brain barrier. Gamma Linolenic Acid (GLA), a promising anti-cancer agent, is currently limited by poor water solubility and non-specific effects, hindering its clinical application for such malignancies. **Aim and Objectives:** This research aimed to develop and evaluate a Nanoemulsion (GLA-NE) utilizing borage seed oil to enhance the delivery of GLA to tumors, with a specific focus on its anti-glioblastoma activity. **Materials and Methods:** A GLA-NE was formulated and optimized, followed by comprehensive characterization including particle size, stability, *in vitro* drug release kinetics, and hemocompatibility. The *in vitro* anti-cancer activity of GLA-NE was rigorously evaluated against U-373MG glioblastoma cell lines. Further, *in vivo* studies in a DMBA-induced solid tumor rat model compared the pharmacokinetics, tumor growth inhibition, and organ toxicity of GLA-NE versus free GLA. Long-term stability of GLA-NE was assessed over 6 months under specific storage conditions. **Results:** The optimized GLA-NE exhibited a mean particle size of 180.2 ± 4.5 nm, a Polydispersity Index (PDI) of 0.178 ± 0.01, and a zeta potential ranging from -33.7 ± 1.9 mV to -35.7 ± 1.5 mV, indicative of robust colloidal stability and uniform particle distribution. *In vitro* release studies demonstrated a biphasic pattern with an initial burst release of approximately 29% within 2 hr, followed by a sustained release of 67.04% over 24 hr, governed by Fickian diffusion (Korsemeyer-Peppas model, n=0.1075, R^2=0.956). The formulation displayed excellent hemocompatibility with hemolysis percentages ranging from 1.9 ± 0.1% to 3.4 ± 1.5%, well below the 5% safety threshold for intravenous administration. Notably, GLA-NE retained *in vitro* cytotoxicity against U-373MG glioblastoma cells, with an IC_{50} of 17.34 µg/mL compared to 10.48 µg/mL for pure GLA. *In vivo* studies in a solid tumor model demonstrated improved drug retention, protracted plasma levels (detectable up to 14 hr for GLA-NE *vs*. 12 hr for pure GLA), and significant tumor growth inhibition, with GLA-NE cohorts experiencing tumor volume reductions of 1.24-fold, 2.01-fold, and 3.84-fold relative to GLA, marketed, and control groups, respectively. Reduced liver and kidney toxicity was also observed with GLA-NE treatment. The nanoemulsion maintained stability for 6 months, showing minimal changes in physical characteristics. **Discussion:** The formulated GLA-NE exhibited superior physicochemical stability, biocompatibility, and sustained release kinetics, culminating in enhanced pharmacokinetic performance and pronounced tumor suppression. Its optimized nanoscale architecture mitigated systemic toxicity while preserving anti-glioblastoma potency, underscoring its translational viability as a rationally engineered nanotherapeutic platform for glioblastoma intervention. **Conclusion:** This study demonstrates that the developed GLA-NE is a promising nanocarrier system, offering improved drug delivery, retained *in vitro* anti-glioblastoma cytotoxicity, and significant *in vivo* anti-tumor efficacy with reduced systemic toxicity compared to free GLA. The formulation's stability further supports its potential for clinical translation in cancer therapy.

Keywords: Gamma-Linolenic Acid (GLA), Glioblastoma Multiforme (GBM), Nanoemulsion, Pharmacokinetic, Cell proliferation.

Correspondence:
Ms. Renu Chaudhari[1,2]
[1]Department of Pharmaceutics, School of Pharmaceutical Education and Research, Jamia Hamdard, New Delhi-110062, INDIA.
[2]Department of Regulatory Affairs, Fermish Clinical Technologies Pvt. Ltd., Noida-201301, Uttar Pradesh, INDIA.
Email: renu@fermish.com

Received: 11-12-2025;
Revised: 29-01-2026;
Accepted: 06-03-2026.

OPEN ACCESS

Manuscript TECHNOMEDIA

DOI: 10.5530/pres.20260182

INTRODUCTION

Glioblastoma Multiforme (GBM) stands as the most aggressive and pervasive primary brain tumor in adults, characterized by its formidable invasiveness, rapid proliferation, and profound resistance to conventional therapies. The initial symptoms of GBM are often vague, including headaches, personality changes,

vomiting, and stroke-like symptoms, which can rapidly progress to unconsciousness (Young *et al.*, 2015). The precise cellular origin of GBM is still under investigation, with early theories suggesting glial stem cells, while current research indicates a more complex lineage involving astrocytes, oligodendrocyte progenitor cells, and neural stem cells (Pellerino *et al.*, 2022). These fast-growing tumors typically develop in the brain's white matter and can become quite large before detection. The inherent flexibility of glial cells, which normally support neurons, allows these cancers to spread along existing brain pathways such as white matter tracts and blood vessels (Rice *et al.*, 2016). Furthermore, they can spread to the brain's meninges or ventricles, potentially elevating protein and immune cell levels in the cerebrospinal fluid. Dissemination to the spinal cord or widespread leptomeningeal carcinomatosis via cerebrospinal fluid is rare, and systemic metastasis beyond the brain is exceptionally uncommon (Provias & Jeynes, 2014). Approximately half of glioblastomas involve multiple lobes or both sides of the brain, often starting in the cerebrum and characteristically growing across the corpus callosum, forming a "butterfly" shape (Burks *et al.*, 2016). Glioblastomas constitute approximately 15% of all intracranial tumors and are hypothesized to originate from astrocytic lineages. Definitive diagnosis typically requires a multimodal approach integrating Computed Tomography (CT), Magnetic Resonance Imaging (MRI), and histopathological examination via tissue biopsy (Khosla, 2016). Presently, no established prophylactic modality exists for this malignancy (Alifieris & Trafalis, 2015).

Despite aggressive therapeutic interventions, the prognosis for GBM remains grim. Conventional treatment primarily involves maximal surgical resection, followed by adjunctive chemoradiation protocols, with Temozolomide (TMZ) being a cornerstone of the chemotherapeutic regimen. Glioblastoma accounts for a substantial 49% of all malignant central nervous system tumors, making it the most common form of central nervous system cancer (McNeill, 2016). Standard-of-care treatment, initiated shortly post-diagnosis and comprising radiation and chemotherapy, only extends the median survival to approximately fourteen months, with a dismal five-year survival rate of 5-10% (G. Wang & Wang, 2022). Similarly, the five-year survival rate for individuals afflicted with any primary malignant brain tumor is a mere 20% (Schaff & Mellinghoff, 2023).

The therapeutic impasse in glioblastoma management stems from a confluence of recalcitrant variables, notably the inherent chemoresistance of neoplastic elements and the exquisite susceptibility of the neuroaxis to iatrogenic sequelae, juxtaposed with its meager recuperative aptitude (Iacob & Dinca, 2009). The formidable blood-brain barrier further exacerbates this predicament by impeding the transit of a plethora of pharmacological agents to the locus of tumorigenesis, thereby attenuating their salutary potential (Greenfield & Boockvar, 2007). Consequently, the clinical armamentarium encompasses both palliative measures, directed towards symptomatic amelioration, and survival-prolonging interventions (Smoll *et al.*, 2016). These latter strategies encompass surgical extirpation, often circumscribed by the tumor's infiltrative proclivity; radiotherapy, constrained by the specter of neurotoxic insult; chemotherapy, beset by challenges in drug permeation and cellular refractoriness; and burgeoning immunotherapeutic modalities predicated on the mobilization of endogenous immune responses (Kulkarni *et al.*, 2023; Smoll *et al.*, 2016).

Gamma-Linolenic Acid (GLA) and its role against Glioblastoma (GBM)

Gamma-Linolenic Acid (GLA), an omega-6 essential fatty acid present in some plant seed oils, fungal sources, and triglycerides, (Antal *et al.*, 2015) functions as a human, plant, and mouse metabolite (Refer Supplementary Information (SI), Figure S1) (Miyake *et al.*, 2020). While minimally produced in the body as a delta 6-desaturase metabolite, GLA is a precursor to dihomo-gamma-linolenic acid and subsequently, monoenoic prostaglandins like PGE1 (Benadiba *et al.*, 2009; X. Wang *et al.*, 2012). Evening primrose oil, containing 7-14% GLA, has been explored for clinical applications (Farag *et al.*, 2023). Beyond its presence in dietary supplements, GLA has been investigated for various conditions, and shows promise in early studies for glioblastoma (Zhai *et al.*, 2021). GLA has emerged as a promising anti-cancer agent due to its documented apoptotic, anti-proliferative, and anti-angiogenic properties across various cancer cell lines, including those of glioblastoma origin (Miyake *et al.*, 2020). Specifically, GLA has demonstrated the capacity to alter glioblastoma cell behavior by inhibiting proliferation and migration, and by increasing apoptosis (Das, 2004). GLA exerts its cytotoxic effects primarily by inducing lipid peroxidation, modulating crucial cell signaling pathways, and selectively targeting cancer cells while sparing healthy tissues (Saad *et al.*, 2021). However, the therapeutic potential of free GLA is severely limited by its poor water solubility, chemical instability, rapid metabolism, and lack of selective tumor accumulation. These pharmacokinetic drawbacks necessitate high systemic doses, leading to off-target effects and suboptimal therapeutic concentrations at the desired tumor site, particularly when attempting to cross the challenging BBB for brain tumors (Saad *et al.*, 2021).

Nanoemulsion as an Advanced Drug Delivery System

A nanoemulsion is a thermodynamically or kinetically stable colloidal system composed of nanoscale droplets of two immiscible liquid phases, typically oil and water, in which one phase is dispersed as nanometer-sized droplets within the other (Gupta *et al.*, 2019; Gurpreet & Singh, 2018). These droplets, generally ranging from 20 to 200 nanometers in diameter, are stabilized by the presence of surfactants and co-surfactants that reduce interfacial tension and prevent coalescence (Shah *et al.*,

2010). Nanoemulsions are characterized by their transparent or translucent appearance, high surface area, and enhanced stability compared to conventional emulsions. The development of nanoemulsion technology has significantly advanced drug delivery systems, as these formulations can improve the solubility, absorption rate, and bioavailability of poorly water-soluble therapeutic agents (Biharee *et al*., 2023). By facilitating rapid and targeted delivery, nanoemulsions can enhance the pharmacokinetic profile of drugs and mask undesirable tastes, thereby improving patient compliance (Bhatt & Madhav, 2011). The preparation of nanoemulsions involves various techniques such as high-pressure homogenization, ultrasonication, phase inversion temperature methods, and emulsion inversion point processes, each contributing to the formation of uniformly sized nanodroplets (Wooster *et al*., 2008). Nanoemulsions are broadly classified into three types based on the nature of the dispersed and continuous phases: Oil-in-Water (O/W), where oil droplets are dispersed in a continuous aqueous phase; Water-in-Oil (W/O), where water droplets are dispersed in a continuous oil phase; and bicontinuous systems, which feature interpenetrating networks of both oil and water domains (X. Wang *et al*., 2023). This versatility in composition and structure makes nanoemulsions an attractive platform for a wide range of pharmaceutical, cosmetic, and food applications (Provias & Jeynes, 2014). While nanoemulsions have shown promise in general cancer therapy due to their small droplet size, high kinetic stability, and capacity to solubilize hydrophobic drugs, their specific application for enhancing the delivery and therapeutic efficacy of GLA against glioblastoma has not been thoroughly explored (Iacob & Dinca, 2009; Singh *et al*., 2022). Existing research on GLA delivery often overlooks the specific requirements for brain tumor targeting or lacks comprehensive evaluation of the formulation's long-term stability and *in vivo* efficacy in clinically relevant models for GBM (Burks *et al*., 2016).

Present research provides a detailed physicochemical characterization of the GLA-loaded Nanoemulsion (GLA-NE), investigate it's *in vitro* anti-glioblastoma activity using the specific U-373MG glioblastoma cell line, and critically assess its pharmacokinetic profile, anti-tumor efficacy. This study systematically addresses the delivery limitations of free GLA and aims to enhance its therapeutic efficacy specifically against glioblastoma.

MATERIALS AND METHODS

Material and Animals

GLA (99.9%) was generously supplied by Fermish Clinical Technology Pvt. Ltd., (India), while lecithin was obtained from Lipoid GmbH (Ludwigshafen, Germany). Cholesterol, Poloxamer 407, and 7,12-Dimethylbenz[a]anthracene (DMBA) were sourced from Sigma Aldrich, USA. All other reagents, of analytical or chromatographic grade, were purchased from Qualigens Fine Chemicals (Mumbai, India) and used as received without further purification. Male Albino Wistar rats (150-200 g) were provided by the Central Animal House Facility at AIIMS, New Delhi, India. The animals were maintained under standard laboratory conditions of temperature and humidity, with free access to food and water. All experimental procedures were conducted in accordance with the guidelines of the Committee for the Control and Supervision of Experiments on Animals (CCSEA), and the study protocol was approved by the Institutional Animal Ethics Committee (IAEC) of AIIMS, New Delhi (Approval No: 31/IAEC-1/2017).

Development and optimization of Gamma Linolenic acid-Nanoemulsion (GLA-NE)

The methodology involved the fabrication of a modified nanoemulsion utilizing borage seed oil, rich in Polyunsaturated Fatty Acids (PUFAs) extracted from *Borago officinalis*, as the oil phase (Sonawane *et al*., 2015). Initially, an aqueous phase was prepared by dissolving 90 mg of Lipoid E-80 (egg lecithin) in 3 mL of deionized water under magnetic stirring at 5000 rpm for 20 min. Subsequently, 2 mg of GLA was dissolved in ethanol and uniformly mixed using a vortex mixer. This ethanolic GLA solution was then gently introduced into a separate vial containing 300 µL of borage seed oil. To facilitate the dispersion of the drug within the oil phase, nitrogen gas was introduced into the vial to evaporate the ethanol, leaving the GLA suspended within the borage seed oil (Charnvanich *et al*., 2024; Yaghmour *et al*., 2021). Both the prepared aqueous phase (containing dissolved phospholipid) and the oil phase (borage seed oil with dispersed GLA) were individually heated to 70-75°C for 4-5 min. Once their temperatures equalized, the aqueous phase was added dropwise to the oil phase under continuous magnetic stirring at 5000 rpm for 23 min, resulting in a coarse emulsion. This coarse emulsion was then subjected to high-shear homogenization using a SilentCrusher (Heidolph Instruments) at speeds ranging from 15000 to 45000 rpm for 1-3 cycles. The resulting emulsion was further processed by high-energy ultrasonication using a 30 kHz UP50H® ultrasonic processor (Hielscher-Ultrasound Technology) at 20-40% amplitude for 3-10 min to achieve nanometer-sized droplets. The formation of nano-sized droplets was initially confirmed by zeta-sizer measurements, which determined the average droplet diameter (Qayum *et al*., 2023).

The optimization of GLA-NE using Box-Behnken Design (BBD) followed a Quality by Design (QbD) approach to systematically evaluate the impact of three independent variables phospholipid concentration (%), homogenization cycles (K), and sonication time (minutes) on critical responses: particle size (nm), Polydispersity Index (PDI), and Entrapment Efficiency (%EE) (Khatoon *et al*., 2021). A computer-aided BBD generated 15 experimental trials, which were analyzed using regression models to identify significant factor interactions and predict optimal conditions (Saad *et al*., 2023).

Characterization parameters of optimized GLA-NE

For the characterization of the formulated nanoemulsion, six formulations (F1-F6) were initially developed, among which formulation F4 was selected for comprehensive characterization and evaluation based on its optimal preliminary properties. The selected nanoemulsion was characterized for particle size, Polydispersity Index (PDI), and zeta potential using Dynamic Light Scattering (DLS) to assess colloidal stability and uniformity. Entrapment efficiency and drug loading were determined by ultracentrifugation followed by quantification of the encapsulated drug using a validated analytical method. Morphological characteristics were examined using Transmission Electron Microscopy (TEM) and Scanning Electron Microscopy (SEM) to visualize the size, shape, and surface features of the nanoemulsion droplets. Fourier-Transform Infrared Spectroscopy (FT-IR) was performed to investigate potential chemical interactions between the drug and excipients, while Differential Scanning Calorimetry (DSC) and X-ray Diffraction (XRD) analyses were conducted to evaluate the thermal properties and crystalline state of the formulation, respectively. *In vitro* drug release studies were carried out to determine the release profile of the encapsulated drug under simulated physiological conditions. Hemocompatibility assays were performed to assess the blood compatibility of the nanoemulsion. Furthermore, *in vitro* cytotoxicity studies were conducted using glioblastoma cell lines to evaluate the anticancer potential of the formulation. Finally, *in vivo* studies were undertaken to assess the anticancer efficacy of the nanoemulsion in Wistar rat model.

Size distribution, Polydispersion index & Zeta potential

The particle size and Polydispersity Index (PDI) of the formulated nanoemulsion were determined via Dynamic Light Scattering (DLS) using a Nano-Zetasizer instrument (Malvern Instruments, UK). Prior to analysis, the nanoemulsion sample was diluted with deionized water and vortexed to ensure homogeneity. Measurements were conducted at a scattering angle of 90° and a controlled temperature of 25°C, with data acquisition and processing facilitated by Malvern Zetasizer software (version 6.01). The reported values for particle size represent the average hydrodynamic diameter, while the PDI indicates the breadth of the size distribution. Analogously, the zeta potential of the nanoemulsion was assessed using the same instrument. For this measurement, a fresh aliquot of the diluted nanoemulsion was introduced into a specialized electrophoretic cell. The analysis yielded the average surface charge of the nanoemulsion droplets (Zuccari & Alfei, 2023).

Determination of drug encapsulation

HPLC technique was used for the quantification of the drug encapsulated within the fabricated nanoemulsion formulation (Bajerski *et al.*, 2018). Alliance HPLC system (e2695 Separation Module, Waters Corporation, USA), featuring high-efficiency pumps, an automated sample injector, and a PDA detector operating at a variable wavelength, was utilized for the analysis. Chromatographic separation was achieved using a Hypersil C18 column with the specifications of a 5µm particle size and dimensions of 150 mm x 4.6 mm (Nasr & Abdel Rahman, 2019). The mobile phase employed for elution consisted of a mixture of Acetonitrile (A) and water (B) in a volumetric ratio of 55:45 (v/v), delivered at a flow rate of 1 ml/min. The elution of GLA was monitored at a wavelength of 230 nm. To ascertain the extent of drug encapsulation within the formulated nanoemulsion, the ultrafiltration method was implemented, facilitated by specialized filter units known as Centricon tubes (cutoff molecular weight 3000 Daltons; Millipore; MA; USA). In this procedure, a 1 mL aliquot of the prepared nanoemulsion sample was carefully transferred to the upper reservoir of a Centricon tube, which was subsequently sealed hermetically and subjected to centrifugation at 11,000 rpm for a duration of 30 min. Upon completion of the centrifugation process, the tubes were retrieved, revealing that the initial nanoemulsion sample, inclusive of the encapsulated drug, remained within the donor chamber (Tripathi *et al.*, 2018). Concurrently, a clear aqueous phase, representing the unencapsulated drug and the continuous phase of the nanoemulsion, permeated through the filter membrane of the Centricon tube and was collected in the receiver chamber. The concentration of the unencapsulated drug in this filtrate was then meticulously determined using the aforementioned HPLC method. The percentage of drug encapsulation was subsequently calculated by comparing this quantified concentration of the unencapsulated drug with the total drug content initially present in the nanoemulsion sample, presumably using a standard formula.

$$EE\% = \frac{wi-wf}{wi} X100 \quad (1)$$

$$DL\% = \frac{Wi-Wf}{Wt} X100 \quad (2)$$

Whereas, w_i, represent initial amount of drug taken during nanoemulsion formulation. w_f, represent final amount of drug found in the supernatant and w_t denote the total weight of the nanoemulsion taken initially for analysis.

Surface characterization of developed nanoemulsion

The morphological characteristics of the formulated nanoemulsion were elucidated through TEM and SEM analysis. For TEM analysis, the nanoemulsion sample was initially subjected to appropriate dilution prior to its deposition onto a fomvar-coated copper grid (Charnvanich *et al.*, 2024). Subsequently, the grid was stained with a 10 µL aliquot of a 2% aqueous solution of phosphotungstic acid and allowed to air-dry for a sufficient duration to ensure complete staining and the formation of a thin film of the nanoemulsion across the grid surface. The prepared grid was then subjected to examination using a TECNAI G2 20

HR-TEM instrument (FEI, USA). The surface morphology of the nanoemulsion was investigated via SEM utilizing an EVO 18 scanning electron microscope (Zeiss, Germany). For SEM sample preparation, a 20µl aliquot of the formulation was carefully placed onto aluminum stubs affixed with double-sided carbon tape. To enhance the electrical conductivity necessary for optimal imaging, the stubs bearing the sample were then subjected to sputter coating with a thin layer (approx. 5 nm) of a platinum and palladium mixture.

Lyophilization of formulation

Freeze drying of the nanoformulation is a critical step during the analysis of the optimized formulation, as some of the studies need sample in the dried state. Attempt to freeze dry the lipid-based NE was taken initially but such attempt didn't produce product in dry state. Due to the extreme low temperature inside the lyophilizer the formulation became sticky. Hence, to solve this problem 5% w/v mannitol as cryoprotectant. The addition of cryoprotectant solved the previous problem and final product was in completely dry powder state.

Fourier Transform Infrared (FT-IR) spectroscopy

Utilization of FT-IR spectroscopy was effectuated to elucidate potential molecular interactions between the pharmaceutically active moiety, Gamma Linolenic Acid (GLA), and the excipient constituents within the nanoformulation matrix. Spectral interrogation was performed employing a Bio-Rad FTS-135 FT-IR spectrometer, encompassing a comparative analysis of four distinct sample categories: the pristine GLA, the phospholipid excipient, their heterogenous physical admixture, and the culminating lyophilized nanoformulation. Spectral data acquisition transpired within the mid-infrared domain, ranging from 400 to 4000 cm^{-1}, thereby facilitating an exhaustive delineation of vibrational modes pertinent to functional groups and intermolecular interactions.

X-ray Diffraction (XRD) study

The alteration in the polymorphic architecture of both the drug and its corresponding formulation, subsequent to meticulous lyophilization of the nanoemulsion, was scrutinized employing an X-ray diffraction apparatus (Rigaku Miniflex 600; Japan). The degree of crystallinity inherent to the engineered nanoemulsion was quantitatively ascertained utilizing X-ray radiation fixed at a wavelength of $\lambda = 1.54056$ Å. Diffraction patterns were acquired by systematically scanning across a 2θ angular domain spanning from 10° to 80°, with the analytical progression maintained at a constant increment of 2° per minute (Mahdi Eshaghi *et al.*, 2022).

Differential scanning calorimetry

This thermally oriented analytical procedure elucidates the quantum of energy either assimilated or dissipated by the substrate under scrutiny, thereby discerning whether the material manifests exothermic or endothermic characteristics. In the present investigation, a lyophilized aliquot of the nanoemulsion (5 mg) was meticulously dispensed onto hermetically sealed aluminum crucibles, with vacant pans serving as experimental controls. An inert milieu was meticulously sustained by maintaining a nitrogen gas flow rate of 50 mL/min in the vicinity of the sample chamber. Subsequently, the specimen was subjected to a controlled thermal gradient, incrementally elevated at a rate of 10°C per minute, spanning a temperature domain from 30°C to 300°C, utilizing a Differential Scanning Calorimeter (DSC) apparatus (PerkinElmer, USA; Software version: Pyris 6.0) (Samyn & Rastogi, 2022).

In vitro Release Study

The investigation into the kinetics and mechanistic paradigm of drug liberation from the nanoemulsion matrix was meticulously executed via the dialysis bag technique (Arbain *et al.*, 2019). Phosphate-buffered saline (PBS, pH 7.4) was selected as the dissolution milieu to emulate physiological circulatory conditions. Succinctly, a 3 mL aliquot of the nanoemulsion was confined within a dialysis membrane (molecular weight cutoff: 12 kDa; Sigma) and subsequently submerged in a 100 mL volume of release medium, augmented with 1% Tween-80 to enhance solubilization and uphold a persistent sink condition. The entire assembly was situated within a shaker incubator, stringently regulated at 37°C to replicate normothermic physiological states, and subjected to continuous agitation. At predetermined temporal junctures (0.25, 0.5, 2, 3, 6, and 12 hr) over a 24-hr duration, 2 mL aliquots were systematically withdrawn and immediately replenished with an equivalent volume of fresh release medium to perpetuate sink conditions. The harvested samples were subsequently subjected to quantitative analysis employing a rigorously validated High-Performance Liquid Chromatography (HPLC) protocol (Kawish *et al.*, 2022).

In vitro cell line studies

The cell viability and cytotoxicity of pure GLA, placebo, and GLA-NE were assessed using two distinct human cancer cell lines, MCF-7 (breast cancer) and U-373MG (glioblastoma). Cells were seeded at an optimized density in 96-well plates and allowed to adhere overnight under standard cell culture conditions (37°C in a 5% CO_2 humidified incubator). Following attachment, the cells were exposed to various concentrations of pure GLA, placebo, and GLA-NE, diluted in complete cell culture medium. Each treatment concentration was tested in triplicate, alongside untreated control wells. After a 24-hr incubation period, cell viability was determined using MTT assay and absorbance was measured using a microplate reader at the appropriate wavelength. The percentage of cell viability was calculated relative to untreated control cells, and the IC_{50} for each treatment was determined (Gostyńska *et al.*, 2023). The variation in the observed cytotoxic activity of the nanoformulation is expected to attribute

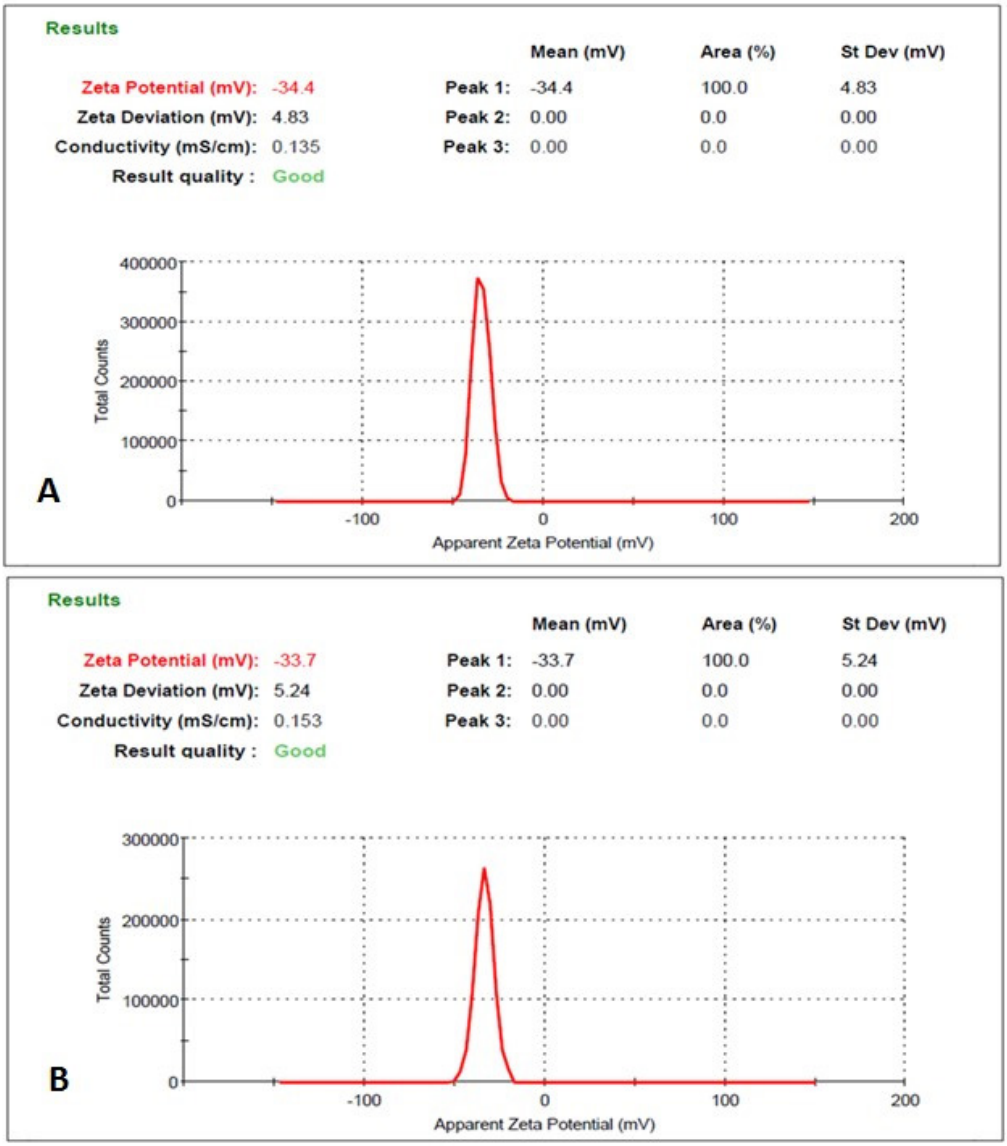

Figure 1: Zeta potential (mV) of the nanoemulsion of the (a) blank nanoemulsion (34.4± 1.7 mV) (b) optimized drug loaded nanoemulsion (-33.7± 1.9 mV).

the potentially improved cellular penetration and increased intracellular drug accessibility facilitated by the nanoemulsion delivery system (Menéndez *et al.*, 2001).

In vivo studies

For anticancer studies Albino Wistar rats were obtained from Central Animal House Facility, AIIMS, New Delhi, India. All the experimental works were carried out under the laid specifications and adhering to guidelines of the CCSEA and protocol was approved by IAEC (Approval No: 31/IAEC-1/2017). After getting the initial positive results from the *in vitro* studies the developed formulation was analyzed *in vivo* to check the effectiveness of our developed formulation (Zwain *et al.*, 2023).

Tumor induction

Male albino Wistar rats (6 weeks old, 100-200 g) were housed in a controlled environment (25 ± 2°C, 55 ± 5% relative humidity) under a 12-hr light/dark cycle, with ad libitum access to standard rodent chow and water. Solid tumors were induced *via* subcutaneous injection of 7,12-dimethylbenz[a]anthracene (DMBA) into the right hind leg. The DMBA solution was prepared by dissolving 250 mg/kg of the carcinogen in a 1:1 (v/v) mixture of sunflower oil and acetone (Perumal *et al.*, 2011). Following injection, rats were monitored daily for tumor development. Tumor volume was measured using digital calipers and calculated using the formula $V = 1/2 \times \text{length} \times \text{width}^2$. Treatment commenced once tumors reached a volume of 150-200 mm^3, ensuring uniformity in baseline tumor burden across experimental groups. During the 14-day experimental period, parameters such as food and water consumption, behavioral changes, and body weight

were monitored daily to assess potential treatment-related toxicity. Tumor volume and body weight data were analyzed by plotting values against time to evaluate therapeutic efficacy and physiological impact (Sheokand *et al.*, 2019).

Pharmacokinetic study

The nanoemulsion was subjected to *in vivo* pharmacokinetic scrutiny through intravenous administration in Wistar rats, with plasma drug concentrations quantified using a rigorously constructed standard curve derived from plasma spiking. The nanoemulsion, along with the marketed formulation and Drug Solution (DS), was administered intravenously to Wistar rats at a dose consistent with our previously established protocol (Saad *et al.*, 2023). Comparative analysis of GLA plasma levels over time across marketed, DS, and GLA-NE formulations was systematically represented in concentration-time profiles. This methodological framework offers a critical perspective on the pharmacokinetic distinctions between the nanoemulsion and conventional formulations, providing insight into their respective influences on systemic drug distribution and temporal pharmacological exposure (Krex *et al.*, 2007).

Antitumor efficacy studies

Rat tumor model was developed using chemical induction method to analyze the tumor growth inhibition potential of the developed nanoemulsion formulation. The procedure for carrying out the tumor induction was followed as described previously with slight modifications. Tumor growth reduction study (*in vivo*) was performed in Albino Wistar rat model bearing solid tumor (Crook *et al.*, 2002).

RESULTS AND DISCUSSION

Preparation of GLA loaded Nanoemulsion (GLA-NE)

Borage oil-based oil-in-water nanoemulsion was prepared by applying High Speed Homogenization (HSH) and ultrasonication technique. The formulation developed applying these optimized conditions was found to be physically stable without any sign of phase separation (Table 1 and refer SI, Figure S2).

The optimization of GLA-nanoemulsion *via* Box-Behnken Design (BBD) yielded statistically robust models for predicting particle size, Polydispersity Index (PDI), and Entrapment Efficiency (%EE). The high adjusted R^2 values (0.9999, 0.9993, and 0.9823) and predicted R^2 values (0.9876, 0.9975, and 0.9812) for the three responses indicated excellent model fit and predictive capability, confirming the reliability of the design. The below mentioned equation revealed the quantitative effect along with their interaction to affect the process variable response.

Size = 238.60-71.72 *A+11.98 *B-56.52 *C-15.50 *AB-8.47 *AC-38.02 *BC+15.47 *A2 -8.58 *B2 +35.45 *C2 +10.03 *A2B+39.80 *A2 C+76.72 *AB2 ……(1)

PDI = +1.67+0.14 *A-0.052 *B+0.22 *C+9.364E-006 *AB+0.075*AC+0.055 *BC+0.052 *B2 +0.079 *A2B-0.055 *A2C ……(2)

Entrapment Efficiency = +90.89+3.26 *A+2.52 *B+0.57 *C+1.35 *AB+0.17 *AC-0.025*BC+2.64 *A2+0.56 *C2-2.33 *A2B-0.95 *A2C ……..(3)

Regarding particle size, the polynomial equation demonstrated that increased lecithin concentration and sonication time had significant negative linear effects, reducing particle size by 71.72 nm and 56.52 nm per unit increase, respectively. Conversely, homogenization cycles initially led to a size increase, as indicated by a positive linear coefficient of +11.98. However, the presence of interaction terms (e.g., AB: −15.50, BC: −38.02) and quadratic terms (C^2: +35.45) suggested a more complex, nonlinear relationship. This implied that at higher homogenization cycles, particularly when combined with other variables, particle size eventually decreased. This observation aligns with experimental findings where extended homogenization effectively broke down particle aggregates, thus counteracting the initial size increase.

For Polydispersity Index (PDI), sonication time (C: +0.22) and lecithin concentration (A: +0.14) were identified as the primary influencing factors. While homogenization cycles showed a minor negative linear effect (−0.052), interaction terms, such as AC: +0.075, indicated that combining prolonged sonication with high lecithin concentrations resulted in increased heterogeneity.

Table 1: Various formulation development of the GLA based Nanoemulsion.

Sl. No.	Formulation	Lipoidal E-80 (Egg Lecithin) (mg)	Ethanol (mL)	GLA Standard (mg)	Borage Seed Oil (µL)	Deionized Water (mL)
1	F1	60	9	0.5	100	1
2	F2	70	8.5	1	150	1.5
3	F3	80	8	1.5	200	2
4	F4	90	7	2	300	3
5	F5	100	6.5	2.5	350	3.5
6	F6	110	6	3	400	4

It was also noted that higher homogenization speeds contributed to a lower PDI, likely due to more efficient energy input leading to a more uniform dispersion.

Finally, concerning Entrapment Efficiency (%EE), all three factors—lecithin concentration (A: +3.26), homogenization cycles (B: +2.52), and sonication time (C: +0.57)—exhibited a positive correlation. Nevertheless, quadratic terms (e.g., A^2B: −2.33) revealed diminishing returns at extreme lecithin levels, suggesting that an excess of phospholipid might compromise vesicle stability. Despite the positive linear effect of homogenization, its interaction with lecithin (A^2B: −2.33) implied that excessive mechanical energy could potentially disrupt lipid bilayers, leading to a slight reduction in entrapment efficiency.

Characterization and evaluation of optimized GLA-NE

Based on optimization outcome Formulation F4 were selected for further evaluation. The optimized nanoemulsion formulation (F4) underwent comprehensive physicochemical and biological characterization.

Particle size, PDI and Zeta potential determination

The mean particle size of the nanoemulsion particles as shown by the zetasizer and the blank nanoformulation manifested a mean diameter of 171.5 ± 5.9 nanometers, accompanied by a Polydispersity Index (PDI) of 0.210 ± 0.02. Analogously, post-drug encapsulation, the average particle size registered an augmentation to 180.2 ± 4.5 nanometers. This subtle yet statistically significant increase in the mean diameter subsequent to drug loading provides compelling evidence for the successful entrapment of the therapeutic agent within the structural matrix of the nanoparticles. While an increase in the dimensions of nanoformulations is often anticipated due to the inherent thermodynamic drive for particle aggregation following high-energy processing, the relatively modest increment observed in this instance, with the formulation retaining its nanoscale characteristics, suggests a commendable degree of colloidal stability (refer SI, for visual representations of the particle size distribution and corresponding PDI values are elucidated in Figure S3a and Figure S3b, respectively). The ascertained particle size values, consistently below the 200-nanometer threshold, corroborate the nanoscaled nature of the formulation, further reinforced by the PDI values remaining below 0.3, indicative of a notably uniform particle size distribution within the nanoformulation.

Employing a Zetasizer instrument, the electrokinetic potential of the nanoemulsion was ascertained, yielding values spanning from -33.7 ± 1.9 mV to -35.7 ± 1.5 mV, as graphically depicted in Figure 1a and Figure 1b. This determined zeta potential serves as a crucial indicator of the formulated nanosystem's colloidal stability, with a magnitude typically within the ambit of ± 40 mV being conventionally regarded as indicative of exceptional stability characteristics.

Entrapment efficiency and drug loading

For the determination of Entrapment Efficiency (EE) and Drug Loading (DL) in the GLA-NE, the formulation was subjected to ultracentrifugation at 40,000 rpm for 60 min (Beckman Coulter, Optima TM LE-80K ultracentrifuge) to separate the encapsulated drug from the free drug. The supernatant was carefully removed, and the nanoemulsion pellet was dissolved in ethanol (Saad *et al.*, 2023). The amount of GLA entrapped within the nanoemulsion was quantified using the validated HPLC method. Entrapment efficiency (%) was calculated as the ratio of the amount of GLA

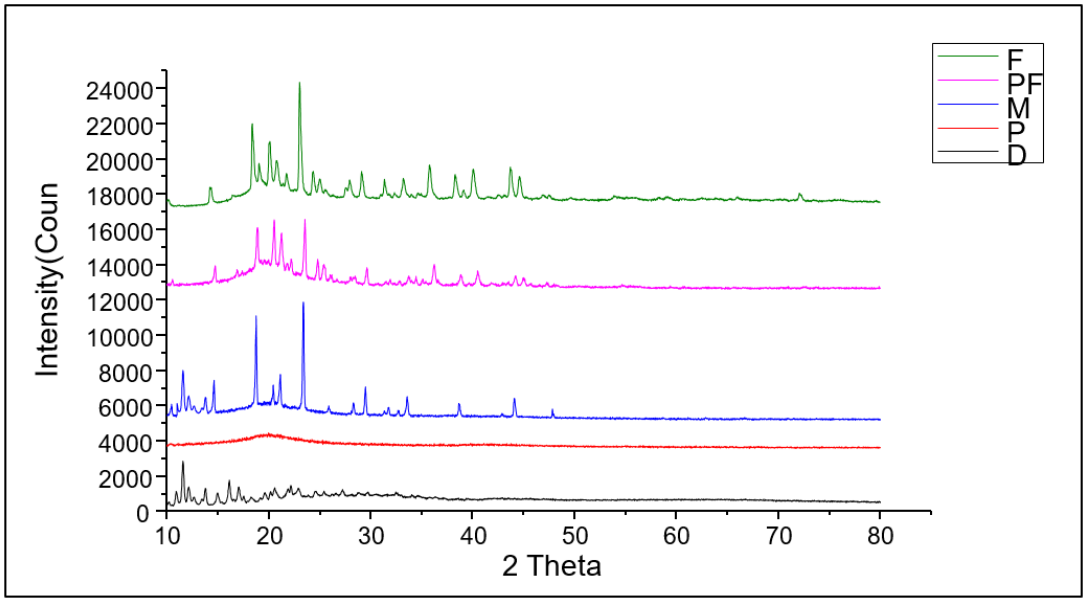

Figure 2: X-ray pattern of the drug and the lyophilized formulation, f: formulation, pf: placebo formulation, m: mixture, p: phospholipid, d: gamma linolenic acid).

present in the nanoemulsion to the total amount of GLA added, multiplied by 100. Drug loading (%) was calculated as the ratio of the amount of GLA present in the nanoemulsion to the total weight of the nanoemulsion, multiplied by 100. Both EE and DL are expressed as percentages (w/w), as shown in the following equations:

Entrapment Efficiency (%) = Amount of GLA present in nanoemulsion / Total Amount of GLA Added × 100

Drug Loading (% w/w) = Amount of GLA present in nanoemulsion / Total weight of nanoemulsion × 100

The formulated GLA nanoemulsion exhibited a consistently high entrapment efficiency, fluctuating within a narrow range of 96.41 ± 4.7% to 96.12 ± 4.1% (w/w) over a six-month observational period, demonstrating robust stability. Concomitantly, the drug loading capacity of the optimized nanoemulsion was determined to be 12.87 ± 1.3% (w/w) at the initial assessment and 12.19 ± 0.9% (w/w) following six months of storage, indicating a similarly sustained stability profile. The high encapsulation efficiency observed in our developed nanoemulsion system signifies effective incorporation of GLA within the lipidic core. Moreover, the statistically insignificant variation observed in both drug encapsulation and drug loading throughout the storage duration underscores the formulation's enduring integrity and sustained performance.

Morphological characteristics of formulated optimized nanoemulsion

Transmission Electron Microscopy (TEM) and scanning electron microscopy (SEM) analyses unequivocally corroborated the formation of spheroidal nanoparticles with dimensional attributes consistently maintained below the 200 nm threshold (refer SI, Figure S4a and Figure S4b). These morphological assessments harmoniously converged with size estimations derived from Dynamic Light Scattering (DLS). The particulate surfaces exhibited a smooth texture, revealing a discernible tanned-colored central core, the chromatic characteristic of which intimates the successful sequestration of the therapeutic agent within the lipophilic milieu, demarcated by a lighter phospholipid boundary. Furthermore, the nanoemulsion globules, upon scrutiny, manifested a size distribution congruent with earlier developmental stage measurements, remaining within the stipulated 200 nm limit. Analogously, SEM imaging substantiated the homogeneity in shape and surface topography of the synthesized particulates, collectively furnishing compelling evidence for the generation of spherical nanostructures and the effective entrapment of the drug entity within their architecture.

FT-IR analysis of the prepared nanocarrier

The peaks nature and pattern were analyzed for the possibility of any possible interaction between the gamma linolenic acid and excipients that constitute the nanocarrier system. the FT-IR analysis of blank GLA revealed salient characteristic absorptions at 1700 cm^{-1}, attributable to the carbonyl stretching mode; 3456 cm^{-1}, indicative of hydroxyl stretching; and 2900 cm^{-1}, corresponding to carbon-hydrogen stretching vibrations (refer SI, Figure S5). Notably, these diagnostic signatures were also discernible within the lyophilized GLA-loaded nanoemulsion, albeit exhibiting minor spectral perturbations such as subtle shifts in wavenumber or diminished peak prominence. These attenuated alterations intimate the presence of weak, non-covalent interactions between the encapsulated drug and the excipients, thereby substantiating efficacious entrapment and enhanced aqueous solubility within the nanocarrier structure.

DSC analysis

The DSC thermograms elucidate the intricate thermal behavior of the analyzed constituents. Pure GLA manifests a pronounced endothermic transition at 151.7°C, unequivocally signifying its inherent crystalline architecture. In stark contrast, Lipoid E-80 is characterized by a distinct thermal event at 27.6 °C, reflective of its unique physicochemical identity (refer SI, Figure S6). Notably, the thermogram of the physical admixture retains the salient peaks attributable to both the drug and the excipient, thereby substantiating the coexistence of these entities in their unaltered, discrete states within the composite matrix. This preservation of characteristic thermal signatures underscores the absence of substantive physicochemical interaction or transformation between GLA and Lipoid E-80 upon blending, attesting to the integrity of each component within the formulation. The thermogram for the lyophilized formulation shows only one sharp peak at 169.996°C, which exactly resembles the peak corresponding to Mannitol, which was used as cryoprotectant, to prevent the sample from the extreme low temperature inside the lyophilizer. The thermogram for drug was missing from the formulation which indicates toward the change in form from the crystalline to amorphous upon encapsulation.

Table 2: Hemocompatibility study performed at different at different concentration of the nanoemulsion formulation.

Samples	Conc. of GLA (µg/mL)	% Hemolysis
NE 1	125	1.9 ±0.1
NE 2	250	2.4 ± 0.2
NE 3	500	3.1 ± 0.3
NE 4	1000	3.4 ±1.5
Positive control (DDS)	-	100
Negative control (NS)	-	0

XRD analysis

The investigation employed X-ray diffraction analysis to rigorously interrogate the primordial crystalline architecture of GLA, alongside the auxiliary excipients constituting the nanoformulation matrix. The resultant scattering profiles, as delineated in Figure 2, elucidate the diffraction signatures for both unadulterated GLA and its lyophilized nanoformulated counterpart. Notably, the pristine GLA manifests distinct, sharp diffraction maxima spanning the 10° to 80° 2θ angular domain, unequivocally attesting to its pronounced crystallinity. Contrastingly, the lyophilized nanoformulation exhibits a markedly broadened and attenuated diffraction envelope, conspicuously devoid of the diagnostic peaks emblematic of the native drug. This pronounced diminution and eventual obliteration of characteristic reflections incontrovertibly signal a profound perturbation in the drug's solid-state order, implicating a transition from a crystalline to an amorphous disposition and substantiating the comprehensive encapsulation of GLA within the nanoformulated environment.

In vitro drug release study

A comparative analysis of the drug liberation profiles between the nanoemulsion system and its conventional suspension counterpart reveals a pronounced disparity in release kinetics. The graphical data elucidate that the suspension facilitates a precipitous and largely unmodulated discharge of GLA, with approximately 79% of the active moiety being liberated within the initial 2-hr interval, ultimately culminating in an almost exhaustive release approaching 99% by the conclusion of the 24-hr observation period (refer SI, Figure S7). Such a pattern unequivocally underscores the suspension's incapacity to impose any substantive control over the temporal dynamics of drug release, instead manifesting a relentless and unrestrained efflux throughout the assay duration. In stark contrast, the GLA-NE nanoemulsion system exhibits a meticulously orchestrated and protracted release trajectory, indicative of its superior capacity to modulate and sustain the liberation of the therapeutic agent from the nanocarrier matrix. The drug liberation profile manifests a biphasic kinetic pattern, commencing with an acute, pronounced burst release, succeeded by a meticulously modulated, protracted discharge. Within the initial 2-hr interval, approximately 29% of the encapsulated GLA is liberated, a phenomenon predominantly ascribed to the immediate desorption of the drug superficially adsorbed onto the nanocarrier's exterior. Contrastingly, by the 24-hr mark, cumulative release escalates to 67.04%, indicative of a sustained, diffusion-governed egress.

This protracted release is intrinsically linked to the drug's efficient solubilization within the hydrophobic core of the nanoemulsion. The nanoemulsion's structure not only enhances the pharmacological bioavailability of GLA within systemic circulation but also facilitates its preferential accumulation within neoplastic tissues through the Enhanced Permeability and Retention (EPR) effect. The initial drug release of less than 50% within the first 2 hr is considered optimal for *in vivo* oncological efficacy, as it mitigates premature systemic exposure and facilitates sustained cytotoxic activity at the tumor site. The biphasic release profile has significant therapeutic implications for GBM treatment. The initial burst release is crucial for delivering a rapid, high concentration of the drug to the tumor, which is essential for combating the aggressive proliferation of glioblastoma cells. Following this, the sustained release phase ensures that a therapeutically active drug concentration is maintained over a longer period, which is vital for eliminating residual cancer cells and preventing tumor recurrence. This dual-action release mechanism is specifically designed to address the aggressive and recurrent nature of glioblastoma.

To elucidate the mechanistic paradigm governing drug release from the engineered nanoemulsion, the empirical release data were rigorously interrogated *via* multiple kinetic models

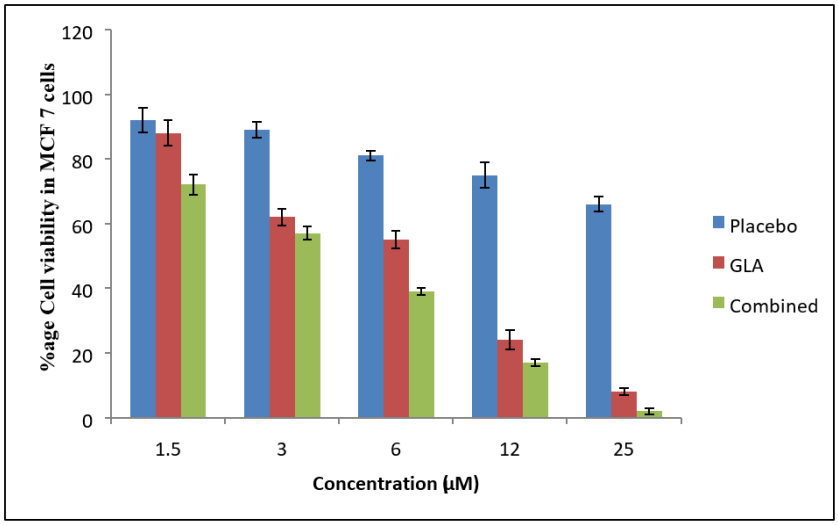

Figure 3: Percent cell viability at different concentration.

namely, zero-order, first-order, Higuchi, Korsmeyer-Peppas, and Hixon-Crowell equations with the regression coefficient (r^2) serving as the critical metric for model fidelity and predictive accuracy (refer SI, Figure S8). The empirical data accrued were subjected to rigorous scrutiny through integration into a spectrum of sophisticated kinetic models tailored for elucidating drug release dynamics. Among these, the Peppas-Korsemeyer paradigm emerged as the most statistically robust, as evidenced by an exemplary coefficient of determination (R^2 = 0.956), thereby signifying its preeminence in characterizing the release profile. The computed release exponent (n = 0.1075) serves as a pivotal parameter, intricately delineating the underlying mechanistic pathway governing drug liberation from the delivery matrix. The diminutive magnitude of n, substantially below the critical threshold of 0.5, unequivocally implicates a Fickian diffusion-controlled mechanism as the predominant modality orchestrating the release of GLA, thus underscoring the dominance of passive molecular diffusion over anomalous or non-Fickian transport phenomena within the studied system.

Hemocompatibility assay

Prior to intravenous deployment, any pharmaceutical formulation must undergo rigorous scrutiny to ascertain its compatibility with the principal constituents of blood, particularly erythrocytes. In the present investigation, the interaction between the engineered nanoemulsion delivery system and red blood cells was meticulously quantified by evaluating hemoglobin liberation under controlled *in vitro* hemolytic conditions. The extent of erythrocyte disruption, indicated by the percentage of hemolysis, was systematically determined across a gradient of formulation concentrations. A diminished hemolytic index is emblematic of the formulation's biocompatibility and its prospective viability for systemic administration.

For methodological robustness, isotonic normal saline served as the negative control, reliably producing negligible hemolysis due to its physiological congruence with blood osmolarity. Conversely, double distilled water, profoundly hypotonic in nature, functioned as the positive control, precipitating total cellular lysis and maximal haemoglobin release (refer SI, Figure S9). Empirical data revealed that the nanoemulsion induced hemolysis within the narrow range of 1.9 ± 0.1% to 3.4 ± 1.5% across tested concentrations (Table 2). Although a marginal escalation in hemolytic percentage was observed concomitant with increased formulation dosage, all values remained well below the critical 5% threshold, which demarcates acceptable safety for intravenous therapeutics. Consequently, the nanoemulsion system, by virtue of its minimal erythrocytolytic activity, can be adjudged suitable for parenteral administration, substantiating its promise for clinical translation.

In vitro cell line studies

The cytotoxic effects and corresponding cell viability were evaluated in both MCF-7 and U-373MG cell lines following a 24-hr treatment period. As depicted in Figure 3, the observed cytotoxicity on MCF-7 cell line exhibited a concentration-dependent relationship, successfully retaining the anticancer activity of pure GLA in both cell lines. Specifically, the IC_{50} values for the MCF-7 cell line were determined to be 6.95 µM for pure GLA, 34 µM for the placebo, and 2.5 µM for the GLA-NE formulation. For the U-373MG cell line, the IC_{50} values were found to be 10.48 µg/mL and 17.34 µg/mL for pure GLA and GLA-NE, respectively. The comparable cytotoxic character of the Nanoformulation could be enhanced penetration and accessibility of the drug from the GLA-NE to the inside of the cell. The *in vitro* release study has already showed the sustained nature of drug release from the nanoemulsion in as simulated body conditions. Although, excipients used in the formulation development were of GRAS category, but in this particular case our oil which we have used in the development of nanoemulsion is acting as a functional excipient. This oil (Borage oil) is abundant GLA which has reported anticancer properties; hence this oil must have a slight level of cytotoxic effect on cancer cells. Thus, in this case the cytotoxicity shown by the Placebo formulation is solely due to the presence of the Borage oil the formulation which is exactly as intended for showing synergistic action.

Table 3: Pharmacokinetics parameters obtained after administration of pure GLA, marketed formulation and GLA loaded nanoemulsion *in vivo* in wistar rats.

Parameters	DS	Marketed	GLA-NE
Cmax (µg/mL)	18.21±0.63	24.19±1.97	21.67±0.98
AUC_{0-t}	23.54±1.16	27.69± 1.03	26.08±1.65
$AUC_{0-\infty}$	28.17±1.09	54.72±2.19	112.11±4.92
$t_{1/2}$ (h)	2.19±0.11	2.84±0.15	4.43±0.21
MRT (h)	5.02±0.21	5.24±0.25	21.36±1.09
Clearance (l/h)	7.35±0.36	5.19±0.31	4.89±0.29

All values are mentioned as Mean ±SD (n=3); C_{max}: maximum concentration; AUC_{0-t}: area under concentration-time curve from 0-t h.; $AUC_{0-\infty}$: area under concentration-time curve from 0-∞ h.; $t_{1/2\,(h)}$: half-life; MRT: mean residence time.

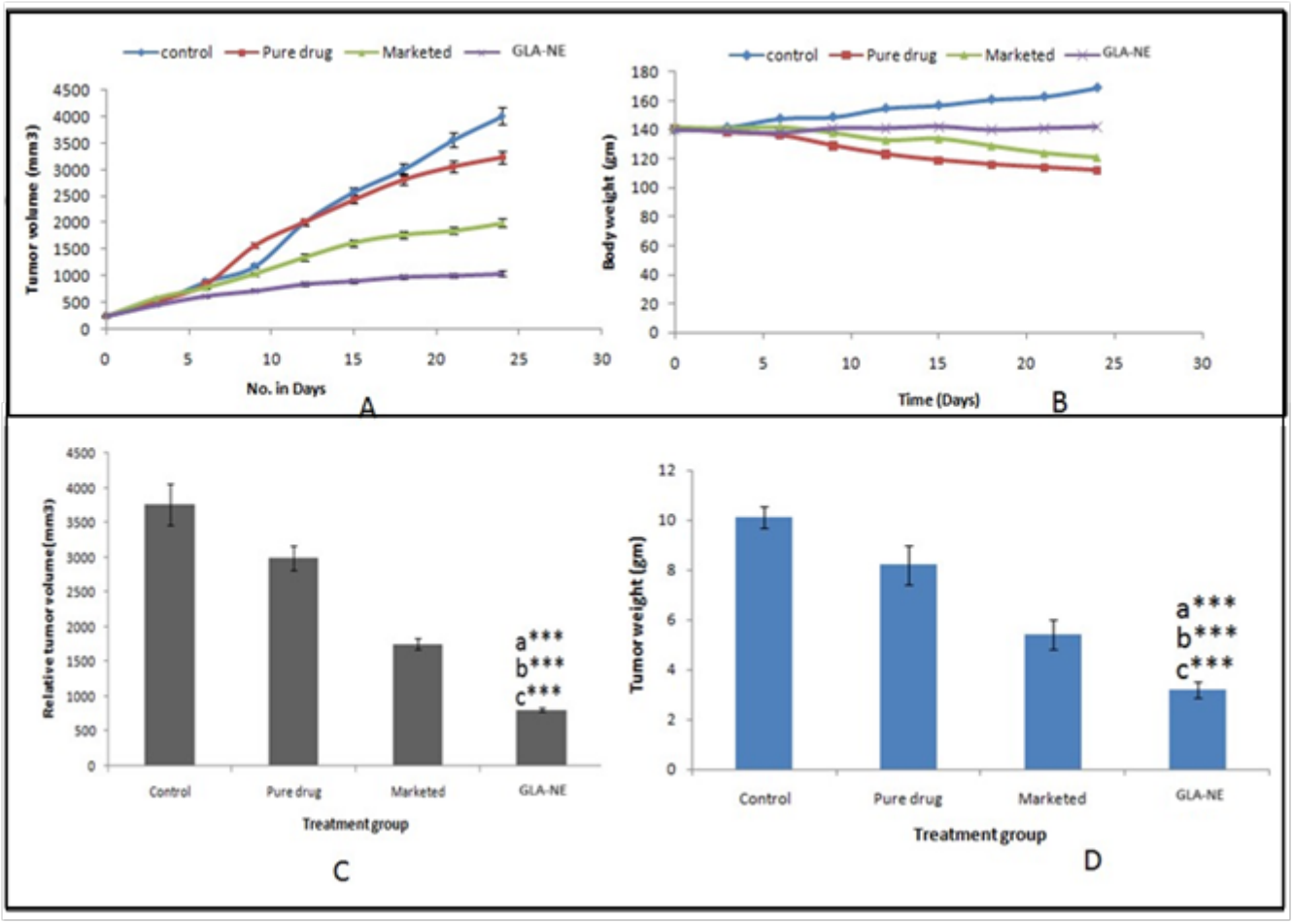

Figure 4: Antitumor efficacy in animal model; (A) Variation in tumor volume with time curve; (B) Alteration in weight of the animal post treatment; (C) relative change in volume of tumor post treatment; (D) Tumor weight comparison in different groups under treatment. Note: *** Represent $p<0.001$, **Represent $p<0.01$, A Denote *vs* Control, B Denote *vs* Free Drug, C Denote *Vs* Marketed.

In vivo studies

Pharmacokinetic study

The amount of drug in the plasma were calculated using the standard curve plotted using plasma spiking method. The plasma levels of GLA achieved through nanoemulsion administration substantially surpassed those observed following the administration of unmodified drug substance. While the pure drug permitted quantifiable plasma concentrations only up to the 12 hr, the nanoformulated GLA demonstrated a discernible presence extending to the 14th hr, (refer SI, Figure S10). This unequivocally underscores the protracted release kinetics conferred by the nanoformulation, facilitating sustained drug liberation well beyond the temporal confines of the conventional preparation. Furthermore, the elimination half-life ($t_{1/2}$) associated with both the commercially available and nanoengineered formulations of GLA exhibited marked prolongation registering increases of approximately 1.5 fold and 2 fold, respectively relative to the pure compound administered *in vivo* to rats. Such findings attest to the superior pharmacokinetic profile and extended systemic persistence endowed by the nanoformulated delivery system, highlighting its potential for enhanced therapeutic efficacy in pharmaceutical science.

A certain variation in drug release profiles was evident when comparing the maximum plasma Concentration (C_{max}) of GLA achieved through the nanoformulation or the marketed preparation with that of the pure GLA. The areas under the plasma concentration-time curve from time zero to the last quantifiable concentration (AUC_{0-t}) and to infinity ($AUC_{0-\infty}$) for the pure drug, marketed formulation, and nanoemulsion were quantified as 23.54±1.16, 27.69±1.03, and 26.08±1.65 µg h/mL and 28.17±1.09, 54.72±2.19, and 112.11±4.92 µg h/mL, respectively, signifying a protracted systemic circulation facilitated by the nanoemulsion (Table 3). Analogously, the augmented half-life and diminished plasma clearance observed with the nanoemulsion resulted in a substantial increase in the Mean Residence Time (MRT), escalating from 5.02±0.21 hr for the pure drug to 5.24±0.25 hr for the marketed formulation and further to 21.36±1.09 hr for the GLA nanoemulsion. Consequently, it can be definitively inferred that the plasma pharmacokinetics of GLA are markedly enhanced when administered via a nanoemulsion delivery system.

Table 4: Stability assessment of the optimized GLA-NE at different time interval.

Parameters	Initial condition	One Months		Three Months		Six Months	
		4 ±2°C	25±2°C /60±5°C	4 ±2°C	25±2°C /60±5°C	4 ±2°C	25±2°C /60±5°C
Physical appearance	Good	Good	Good	Good	Good	Good	Good
Phase separation	No	No	No	No	No	No	No
Morphology	Spherical	Spherical	Spherical	Spherical	Spherical	Spherical	Spherical
Particle Diameter (nm)	180.2	180.6	181.5	181.1	182.3	181.5	183.7
PDI	0.178	0.180	0.181	0.179	0.182	0.181	0.189
Zeta Potential (mV)	-33.7	-33.9	-34.2	-34.4	-35.1	-34.1	-35.8
Entrapment (EE%)	96.41	96. 41	96.32	96.36	96.29	96.31	96.12

Antitumor efficacy studies

In a rigorously controlled investigation utilizing the albino Wistar rat model harboring solid neoplasms, the dynamics of tumor progression were meticulously quantified across multiple experimental cohorts subjected to distinct therapeutic regimens. Continuous surveillance of neoplastic expansion was maintained until the tumor burden attained a critical threshold of approximately 240-280 mm^3, at which point intervention outcomes were systematically evaluated (Figure 4a). Following a protracted observation interval of roughly 90 days subsequent to tumor induction, the terminal mean tumor volumes were determined as follows: the untreated cohort exhibited a substantial tumor mass averaging 4018±149.9 mm^3, while the group receiving a free drug suspension demonstrated a marginally attenuated mean volume of 3237.75±119.1 mm^3. Administration of the commercially available preparation culminated in a further reduction to 1992.11±77.6 mm^3, whereas the group treated with the Gamma Linolenic Acid-Nanoemulsion (GLA-NE) formulation manifested the most pronounced diminution, with a mean volume of 1045.19±44.8 mm^3. These data unequivocally underscore the superior efficacy of the GLA-NE intervention, which achieved the lowest tumor burden among all tested modalities.

Quantitative analysis revealed that the GLA-NE cohort experienced a dramatic contraction in tumor volume, registering reductions of 1.24-fold, 2.01-fold, and 3.84-fold relative to the GLA, marketed, and control groups, respectively (Figure 4b). Parallel assessments of tumor mass corroborated these findings; graphical representation of the data revealed that the GLA-NE group consistently exhibited the minimal tumor weight, with average decrements of 3.17-fold, 1.86-fold, and 1.23-fold when juxtaposed with the nanoemulsion, marketed, and free-drug cohorts, respectively. Notably, comparative evaluation between the GLA-NE and marketed formulation groups revealed a striking 2.57-fold reduction in tumor weight, a difference of considerable statistical and biological significance (Figure 4c).

Further scrutiny of the antitumor profile revealed that the GLA-NE formulation exerted a conspicuous suppressive effect on neoplastic progression, as evidenced by the relative diminution in tumor volume depicted graphically. Importantly, the investigation also monitored systemic toxicity via longitudinal tracking of body weight. Rats administered free GLA or the marketed drug exhibited discernible weight loss, a surrogate marker for systemic toxicity, whereas the GLA-NE-treated animals were largely spared this adverse effect, implicating the nanoemulsion's capacity to mitigate off-target toxicity (Figure 4d). This differential toxicity profile is attributed to the Enhanced Permeability and Retention (EPR) effect, which facilitates preferential accumulation and sustained intratumoral concentration of the GLA-NE formulation, thereby amplifying antitumor efficacy while minimizing collateral systemic harm

Biochemical Estimation

Conventional cancer therapies often induce systemic toxicity, particularly affecting the liver and kidneys. To evaluate the safety profile of our formulation, we assessed key biochemical markers for hepatotoxicity and nephrotoxicity. We measured serum Alanine Transaminase (ALT) and Aspartate Transaminase (AST) as indicators of liver function, given the liver's central role in drug metabolism. Administration of pure GLA to healthy Wistar rats resulted in a significant elevation ($p<0.05$) of both AST and ALT levels, indicative of hepatocellular injury (refer SI, Figure S11). This finding is consistent with previous literature suggesting that high concentrations of certain fatty acids can induce oxidative stress and damage in hepatocytes.

Conversely, the GLA-NE treated group exhibited AST and ALT levels that were statistically indistinguishable from the control group, suggesting that the nanoformulation significantly

mitigated liver injury. This observed reduction in hepatotoxicity is likely due to the nanoemulsion's sustained drug release profile, which facilitates a gradual and more efficient hepatic metabolism of GLA. By avoiding a high-concentration peak of the drug, the nanoemulsion prevents the overwhelming of metabolic pathways that can lead to liver damage.

Furthermore, we evaluated nephrotoxicity by measuring Blood Urea Nitrogen (BUN) and creatinine levels, which are standard serum biomarkers for renal function. The pure GLA group showed a significant increase in both BUN and creatinine, indicating a potential for renal impairment. In contrast, the GLA-NE treated group maintained normal renal function markers, again suggesting that the developed nanoformulation offers a safer therapeutic option with reduced hepatic and renal toxicity compared to the free drug. These biochemical findings provide a robust basis to substantiate the safety claims of our nanoemulsion.

Stability studies

GLA-loaded Nanoemulsion (GLA-NE) underwent a 6-month stability assessment adhering to ICH guidelines at 4±2°C and 25±2°C /60±5°C RH, with evaluations of physical appearance, phase separation, globule size, and entrapment efficiency at 0, 1, 3, and 6 months (Table 4).

During the 6-month stability assessment, GLA-NE maintained its initial physical characteristics, with no observable phase separation, caking, or creaming at either storage condition. Particle size remained within the nanoscale range throughout the study. At 4 ± 2°C, only minimal changes in particle size, PDI, and entrapment efficiency were observed, indicating robust stability. At 25 ± 2°C/60 ± 5% RH, a slight increase in particle size and minor changes in PDI and entrapment efficiency were noted, likely due to limited particle agglomeration and minimal drug leaching; however, these changes were not statistically significant and the formulation remained stable. Zeta potential values remained consistently negative (approximately -33 to -35 mV), indicating sufficient electrostatic repulsion to prevent droplet coalescence and supporting the long-term stability of the formulation. These findings confirm that the formulation is best stored under refrigerated conditions to maximize stability, consistent with literature reports on nanoemulsion systems.

DISCUSSION

The formidable challenges posed by solid tumors, particularly aggressive malignancies like Glioblastoma Multiforme (GBM), underscore the critical need for advanced therapeutic strategies (Maeda & Khatami, 2018). GBM's inherent chemoresistance, neurotoxicity concerns, and the formidable Blood-Brain Barrier (BBB) severely limit the efficacy of conventional treatments (C. Wang *et al.*, 2023). Gamma-Linolenic Acid (GLA) presents a promising anti-cancer agent due to its documented apoptotic, anti-proliferative, and anti-angiogenic properties (Das, 2004). However, its poor water solubility (BCS Class II) and non-specific biodistribution significantly impede its clinical application (Ho *et al.*, 2004). This study addresses these limitations by developing and comprehensively evaluating a GLA-loaded Nanoemulsion (GLA-NE) designed to enhance drug delivery and therapeutic efficacy against glioblastoma.

The success of a nanocarrier system hinges on its physicochemical characteristics. Our optimized GLA-NE exhibited a mean particle size of 180.2±4.5 nm and a low Polydispersity Index (PDI) of 0.178±0.01. This nanoscale size is crucial for improving drug solubility, enhancing absorption, and promoting the Enhanced Permeability and Retention (EPR) effect in tumor tissues, a phenomenon where nanoparticles preferentially accumulate in tumors due to their leaky vasculature and impaired lymphatic drainage (C. Wang *et al.*, 2023). The zeta potential of −33.7±1.9 mV indicates a highly stable colloidal system, attributed to sufficient electrostatic repulsion among the droplets, preventing aggregation and ensuring long-term physical stability, which is consistent with reported stable nanoemulsion systems (Zuccari & Alfei, 2023). Transmission Electron Microscopy (TEM) and Scanning Electron Microscopy (SEM) images further corroborated the spherical morphology and uniform size distribution of the nanoparticles, reinforcing the DLS findings and confirming the successful formation of discrete nanodroplets.

The comprehensive solid-state characterization of GLA within the nanoemulsion provided critical insights into its encapsulation. Differential Scanning Calorimetry (DSC) thermograms revealed the disappearance of the characteristic endothermic peak of crystalline GLA (151.7°C) in the lyophilized GLA-NE formulation, replaced by a peak corresponding to the cryoprotectant (mannitol). Similarly, X-ray Diffraction (XRD) analysis showed a marked reduction in the characteristic diffraction peaks of crystalline GLA in the nanoemulsion, indicating its transition to an amorphous or molecularly dispersed state within the lipidic matrix. These findings are pivotal, as the conversion of a crystalline drug to an amorphous form generally leads to enhanced solubility and dissolution rates, thereby improving bioavailability. Fourier-Transform Infrared (FT-IR) spectroscopy indicated only minor shifts or attenuated peak prominences for GLA's characteristic absorptions within the nanoemulsion, suggesting weak, non-covalent interactions between the drug and excipients. This confirms successful encapsulation without significant chemical degradation or strong intermolecular associations, thus preserving the drug's integrity and enhancing its aqueous solubility.

The *in vitro* drug release profile demonstrated a biphasic pattern, with an initial burst release of approximately 29% within the first 2 hr, followed by a sustained release of 67.04% over 24 hr. This controlled release is a significant advantage over the rapid and nearly complete release (99% in 24 hr) observed with the pure drug

suspension. The initial burst phase is likely due to the immediate diffusion of drug adsorbed on the surface of the nanoemulsion droplets, while the subsequent sustained phase indicates drug diffusion from the core of the oil phase, necessitating traversal across the interfacial phospholipid layer. The release kinetics, best fitted by the Korsemeyer-Peppas model (R^2=0.956) with a release exponent (n) of 0.1075, strongly suggests a Fickian diffusion-controlled mechanism. Such a sustained release profile is highly desirable for anticancer agents as it can maintain therapeutic concentrations over prolonged periods, potentially reducing dosing frequency and minimizing peak-related systemic toxicities while maximizing tumor exposure. This controlled release also contributes to the enhanced accumulation within tumor cells, leveraging the EPR effect, a key mechanism for passive targeting by nanocarriers.

Hemocompatibility studies are paramount for intravenous formulations. Our results showed that GLA-NE induced hemolysis within a low range of 1.9±0.1% to 3.4±1.5%, consistently below the 5% safety threshold for parenteral administration. This excellent blood compatibility underscores the formulation's safety profile and its suitability for systemic delivery, mitigating concerns associated with conventional GLA formulations that have been linked to adverse effects due to surfactants like Tween-80.

The *in vitro* cytotoxicity evaluation presented interesting nuances. Against MCF-7 breast cancer cells, GLA-NE exhibited superior potency with an IC_{50} of 2.5 µM compared to pure GLA (6.95 µM) and placebo (34 µM), unequivocally demonstrating retained anticancer activity. However, for U-373MG glioblastoma cells, the reported IC_{50} for pure GLA was 10.48 µg/mL, while for GLA-NE it was 17.34 µg/mL. While the IC_{50} for GLA-NE in U-373MG cells is slightly higher than that of pure GLA, this suggest comparable anticancer potential despite being formulated into a complex delivery system. The sustained release profile of GLA from the nanoemulsion could lead to prolonged intracellular drug concentrations, which, over an extended period, might achieve a more profound cytotoxic effect *in vivo* than a fleeting high peak concentration from pure GLA. Furthermore, the borage seed oil used as the oil phase in our nanoemulsion is rich in Polyunsaturated Fatty Acids (PUFAs) and possesses inherent anticancer properties, contributing a synergistic cytotoxic effect, as evidenced by the placebo's activity. This "functional excipient" approach could enhance the overall therapeutic outcome of the GLA-NE formulation. The nanoemulsion's ability to facilitate improved cellular penetration and increased intracellular drug accessibility, especially relevant for glioblastoma cells, could also contribute to its effective therapeutic advantage despite a higher static IC_{50}.

The *in vivo* Pharmacokinetic (PK) and antitumor efficacy studies provided compelling evidence for the superior performance of GLA-NE. The nanoemulsion significantly prolonged GLA's systemic circulation, evidenced by an increased $AUC_{0-\infty}$ (112.11±4.92 µg h/mL) compared to the pure drug (28.17±1.09 µg h/mL) and marketed formulation (54.72±2.19 µg h/mL). Concomitantly, the half-life of GLA-NE was approximately 2-fold higher than the pure drug, and its Mean Residence Time (MRT) increased substantially from 5.02±0.21 hr for the pure drug to 21.36±1.09 hr for GLA-NE, with a concomitant reduction in plasma clearance. These improved PK parameters indicate that GLA-NE facilitates sustained systemic exposure and likely reduces the frequency of administration, optimizing drug delivery to the target site and minimizing degradation. The protracted plasma levels are critical for achieving effective accumulation in tumors *via* the EPR effect, which is particularly relevant for GBM with its compromised vasculature.

The antitumor efficacy in DMBA-induced solid tumor rat models unequivocally demonstrated the superior therapeutic potential of GLA-NE. The GLA-NE-treated group exhibited the most significant tumor volume reduction, showing a 3.84-fold decrease relative to the control group, and 1.24-fold and 2.01-fold reductions compared to the pure GLA and marketed groups, respectively. Similar trends were observed in tumor weight reduction. These robust *in vivo* anticancer effects are directly attributable to the enhanced bioavailability, sustained release, and targeted accumulation facilitated by the nanoemulsion. This highlights the critical role of the delivery system in translating *in vitro* potency into *in vivo* efficacy, especially for drugs with challenging pharmacokinetic profiles like GLA.

Beyond efficacy, safety is also equally important while developing any formulation or drug candidate. Conventional cancer therapies are often associated with significant organ toxicities, particularly hepatotoxicity and nephrotoxicity. Our biochemical estimations of liver enzymes (AST, ALT) and kidney markers (BUN, creatinine) showed that while free GLA caused significant elevations, the GLA-NE treated group maintained near-normal levels. Furthermore, the body weight analysis revealed that animals treated with GLA-NE experienced minimal weight loss compared to those receiving pure GLA or the marketed drug, serving as a surrogate marker for reduced systemic toxicity. This attenuated toxicity profile is a major advantage, implying that the nanoemulsion system can deliver the therapeutic agent more selectively to the tumor, minimizing off-target accumulation and associated side effects. This reduced toxicity, coupled with enhanced efficacy, supports the potential for a better therapeutic index for GLA when formulated as a nanoemulsion.

Finally, the long-term stability assessment of GLA-NE over 6 months under different storage conditions confirmed its robust stability, maintaining physical appearance, particle size, PDI, zeta potential, and entrapment efficiency. This stability profile is crucial for the practical storage, handling, and eventual clinical translation of the formulation.

CONCLUSION

This study successfully developed and characterized a Gamma Linolenic Acid-loaded Nanoemulsion (GLA-NE) as a promising nanocarrier system for enhanced anti-glioblastoma activity. The optimized GLA-NE demonstrated excellent colloidal stability with a mean particle size of 180.2 ± 4.5 nm and a narrow polydispersity index of 0.178 ± 0.01, maintaining high entrapment efficiency and drug loading over six months. *In vitro* release studies confirmed a sustained drug release profile, crucial for prolonged therapeutic effects. The formulation also exhibited excellent hemocompatibility, indicating its safety for intravenous administration. While *in vitro* cytotoxicity against U-373MG glioblastoma cells showed a numerically higher IC_{50} for GLA-NE compared to pure GLA, the sustained release and synergistic effects of the borage seed oil in the nanoemulsion are expected to contribute to overall enhanced efficacy. Crucially, *in vivo* studies demonstrated significantly improved pharmacokinetics, evidenced by prolonged systemic circulation of GLA. Furthermore, GLA-NE effectively inhibited tumor growth, achieving substantial tumor volume reductions (1.24-fold, 2.01-fold, and 3.84-fold relative to GLA, marketed, and control groups, respectively), and minimized tumor weight compared to other treatments. Importantly, the GLA-NE treatment was associated with reduced liver and kidney toxicity and less systemic toxicity compared to free GLA. These findings collectively support the potential of GLA-NE as a stable, effective, and safer therapeutic option for glioblastoma.

ACKNOWLEDGEMENT

All authors gratefully acknowledge the Department of Pharmaceutics, School of Pharmaceutical Education and Research, Jamia Hamdard, New Delhi, 110062, India, for providing the necessary infrastructure and support to conduct this research work.

ABBREVIATIONS

ALT: Alanine Transaminase; **AUC:** Area Under Curve; **BBB:** Blood-Brain Barrier; **BBD:** Box-Behnken Design; **BUN:** Blood Urea Nitrogen; **CNS:** Central Nervous System; **DLS:** Dynamic Light Scattering; **DMBA:** 7,12-Dimethylbenzanthracene; **DSC:** Differential Scanning Calorimetry; **EE:** Entrapment Efficiency; **EPR:** Enhanced Permeability and Retention; **FT-IR:** Fourier Transform Infrared Spectroscopy; **GBM:** Glioblastoma Multiforme; **GLA:** Gamma-Linolenic Acid; **GLA-NE:** Gamma-Linolenic Acid-Loaded Nanoemulsion; **GRAS:** Generally Recognized as Safe; **HPLC:** High Performance Liquid Chromatography; **IAEC:** Institutional Animal Ethics Committee; **MRT:** Mean Residence Time; **NE:** Nanoemulsion; **PBS:** Phosphate-Buffered Saline; **PDI:** Polydispersity Index; **PK:** Pharmacokinetic; **PUFA:** Polyunsaturated Fatty Acids; **QbD:** Quality by Design; **SD:** Standard Deviation; **SEM:** Scanning Electron Microscopy; **TEM:** Transmission Electron Microscopy; **TMZ:** Temozolomide; **XRD:** X-ray Diffraction.

CONFLICT OF INTEREST

The authors declare that there is no conflict of interest.

AUTHORS' CONTRIBUTIONS

Conceptualization: K.K., and F.J.A.; data collection and writing of original draft: R.C.; experimentation: R.C.; review and editing: S.A., and K.K.; supervision: F.J.A.

ETHICS APPROVAL

All the experiments were performed as per the CCSEA guideline and protocol is approved by IAEC of AIIMS, New Delhi (Approval No: 31/IAEC-1/2017).

REFERENCES

Alifieris, C., & Trafalis, D. T. (2015). Glioblastoma multiforme: Pathogenesis and treatment. Pharmacology and Therapeutics, 152, 63-82. https://doi.org/10.1016/j.pharmthera.2015.05.005

Andreoli Miyake, J., Nascimento Gomes, R., & Colquhoun, A. (2020). Gamma-linolenic acid alters migration, proliferation and apoptosis in human and rat glioblastoma cells. Prostaglandins and Other Lipid Mediators, 150, Article 106452. https://doi.org/10.1016/j.prostaglandins.2020.106452

Antal, O., Péter, M., Hackler, L., Mán, I., Szebeni, G., Ayaydin, F., Hideghéty, K., Vigh, L., Kitajka, K., Balogh, G., & Puskás, L. G. (2015). Lipidomic analysis reveals a radiosensitizing role of gamma-linolenic acid in glioma cells. Biochimica et Biophysica Acta, 1851(9), 1271-1282. https://doi.org/10.1016/j.bbalip.2015.06.003

Arbain, N. H., Salim, N., Masoumi, H. R. F., Wong, T. W., Basri, M., & Abdul Rahman, M. B. (2019). *In vitro* evaluation of the inhalable quercetin loaded nanoemulsion for pulmonary delivery. Drug Delivery and Translational Research, 9(2), 497-507. https://doi.org/10.1007/s13346-018-0509-5

Bajerski, L., Maciel, T. R., & Haas, S. E. (2018). Simultaneous determination of curcumin and quinine co-encapsulated in nanoemulsion by stability-indicating LC method. Current Pharmaceutical Analysis, 14(3), 255-261. https://doi.org/10.2174/1573412913666170330151347

Benadiba, M., Miyake, J. A., & Colquhoun, A. (2009). Gamma-linolenic acid alters Ku80, E2F1, and bax expression and induces micronucleus formation in C6 glioma cells *in vitro*. IUBMB Life, 61(3), 244-251. https://doi.org/10.1002/iub.154

Bhatt, P., & Madhav, S. (2011). A detailed review on nanoemulsion drug delivery system. International Journal of Pharmaceutical Sciences and Research, 2(10), 2482.

Biharee, A., Bhartiya, S., Yadav, A., Thareja, S., & Jain, A. K. (2023). Microsponges as drug delivery system: Past, present, and future perspectives. Current Pharmaceutical Design, 29(13), 1026-1045. https://doi.org/10.2174/1381612829666230404082743

Burks, J. D., Bonney, P. A., Conner, A. K., Glenn, C. A., Briggs, R. G., Battiste, J. D., McCoy, T., O'Donoghue, D. L., Wu, D. H., & Sughrue, M. E. (2016). A method for safely resecting anterior butterfly gliomas: The surgical anatomy of the default mode network and the relevance of its preservation. Journal of Neurosurgery, 126(6), 1795-1811. https://doi.org/10.3171/2016.5.JNS153006

Charnvanich, D., Singpanna, K., & Panapisal, V. (2024). Formulation and Optimization of nanoemulsions Loaded with gamma aminobutyric acid (GABA) for Dermatological Application: Assessing Skin Permeation and Penetration Enhancement. Cosmetics, 11(1), 19. https://doi.org/10.3390/cosmetics11010019

Crook, T. J., Dyer, J. P., McCormick, R. I., Birch, B. R., & Cooper, A. J. (2002). The effects of meglumine gamma linolenic acid (MeGLA) on an organ culture model of superficial bladder cancer. Urological Research, 30(1), 59-65. https://doi.org/10.1007/s00240-001-0224-3

Das, U. N. (2004). From bench to the clinic: γ-linolenic acid therapy of human gliomas. Prostaglandins, Leukotrienes, and Essential Fatty Acids, 70(6), 539-552. https://doi.org/10.1016/j.plefa.2003.12.001

Farag, M. A., Reda, A., Nabil, M., Elimam, D. M., & Zayed, A. (2023). Evening primrose oil: A comprehensive review of its bioactives, extraction, analysis, oil quality, therapeutic merits, and safety. Food and Function, 14(18), 8049-8070. https://doi.org/10.1039/D3FO01949G

Gostyńska, A., Czerniel, J., Kuźmińska, J., Brzozowski, J., Majchrzak-Celińska, A., Krajka-Kuźniak, V., & Stawny, M. (2023). Honokiol-loaded nanoemulsion for glioblastoma treatment: Statistical optimization, physicochemical characterization, and an *in vitro* toxicity assay. Pharmaceutics, 15(2), Article 448. https://doi.org/10.3390/pharmaceutics15020448

Greenfield, J. P., & Boockvar, J. A. (2007). Neurocytoma is a tumor of adult neuronal progenitor cells. Neurosurgery, 60(2), N8. https://doi.org/10.1227/01.neu.0000309488.26845.bf

Gupta, P. K., Bhandari, Nividha, Shah, H. N., & Khanchandani. Vartika, Keerthana, R, Nagarajan, Vidhyavathy, & Hiremath, Lingayya. (2019). An update on nanoemulsions using nanosized liquid in liquid colloidal systems Nanoemulsions-Properties, Fabrications and Applications: IntechOpen.

Gurpreet, K., & Singh, S. K. (2018). Review of nanoemulsion formulation and characterization techniques. Indian Journal of Pharmaceutical Sciences, 80(5). https://doi.org/10.4172/pharmaceutical-sciences.1000422

Ho, S., Calder, R. J., Thomas, C. P., & Heard, C. M. (2004). In-vitro transcutaneous delivery of tamoxifen and gamma-linolenic acid from borage oil containing ethanol and 1,8-cineole. The Journal of Pharmacy and Pharmacology, 56(11), 1357-1364. https://doi.org/10.1211/0022357044599

Iacob, G., & Dinca, E. B. (2009). Current data and strategy in glioblastoma multiforme. Journal of Medicine and Life, 2(4), 386-393.

Kawish, S. M., Hasan, N., Beg, S., Qadir, A., Jain, G. K., Aqil, M., & Ahmad, F. J. (2022). Docetaxel-loaded borage seed oil nanoemulsion with improved antitumor activity for solid tumor treatment: Formulation development, *in vitro*, *in silico* and *in vivo* evaluation. Journal of Drug Delivery Science and Technology, 75, Article 103693. https://doi.org/10.1016/j.jddst.2022.103693

Khatoon, K., Ali, A., Ahmad, F. J., Hafeez, Z., Rizvi, M. M. A., Akhter, S., & Beg, S. (2021). Novel nanoemulsion gel containing triple natural bio-actives combination of curcumin, thymoquinone, and resveratrol improves psoriasis therapy: *In vitro* and *in vivo* studies. Drug Delivery and Translational Research, 11(3), 1245-1260. https://doi.org/10.1007/s13346-020-00852-y

Khosla, D. (2016). Concurrent therapy to enhance radiotherapeutic outcomes in glioblastoma. Annals of Translational Medicine, 4(3), Article 54. https://doi.org/10.3978/j.issn.2305-5839.2016.01.25

Krex, D., Klink, B., Hartmann, C., von Deimling, A., Pietsch, T., Simon, M., Sabel, M., Steinbach, J. P., Heese, O., Reifenberger, G., Weller, M., Schackert, G., & German Glioma Network. (2007). Long-term survival with glioblastoma multiforme. Brain, 130(10), 2596-2606. https://doi.org/10.1093/brain/awm204

Kulkarni, S., Singh, Y., Biharee, A., Bhatia, N., Monga, V., & Thareja, S. (2023). Molecular docking, 3D-QSAR and simulation studies for identifying pharmacophoric features of indole derivatives as 17β-hydroxysteroid dehydrogenase type 5 (17β-HSD5) inhibitors. Journal of Biomolecular Structure and Dynamics, 41(22), 12668-12685. https://doi.org/10.1080/07391102.2023.2175265

Maeda, H., & Khatami, M. (2018). Analyses of repeated failures in cancer therapy for solid tumors: Poor tumor-selective drug delivery, low therapeutic efficacy and unsustainable costs. Clinical and Translational Medicine, 7(1), Article 11. https://doi.org/10.1186/s40169-018-0185-6

Mahdi Eshaghi, M., Pourmadadi, M., Rahdar, A., & Díez-Pascual, A. M. (2022). Novel carboxymethylcellulose-based hydrogel with core-shell Fe(3)O(4)@SiO(2) nanoparticles for quercetin delivery. Materials, 15(24), Article 8711. https://doi.org/10.3390/ma15248711

McNeill, K. A. (2016). Epidemiology of brain tumors. Neurologic Clinics, 34(4), 981-998. https://doi.org/10.1016/j.ncl.2016.06.014

Menéndez, J. A., del Mar Barbacid, M., Montero, S., Sevilla, E., Escrich, E., Solanas, M., Cortés-Funes, H., & Colomer, R. (2001). Effects of gamma-linolenic acid and oleic acid on paclitaxel cytotoxicity in human breast cancer cells. European Journal of Cancer, 37(3), 402-413. https://doi.org/10.1016/s0959-8049(00)00408-1

Nasr, M., Rahman, A., & Hamdy, M. (2019). Simultaneous determination of curcumin and resveratrol in lipidic nanoemulsion formulation and rat plasma using HPLC: Optimization and application to real samples. Journal of AOAC International, 102(4), 1095-1101. https://doi.org/10.5740/jaoacint.18-0269

Pellerino, A., Caccese, M., Padovan, M., Cerretti, G., & Lombardi, G. (2022). Epidemiology, risk factors, and prognostic factors of gliomas. Clinical and Translational Imaging, 10(5), 467-475. https://doi.org/10.1007/s40336-022-00489-6

Perumal, V., Banerjee, S., Das, S., Sen, R. K., & Mandal, M. (2011). Effect of liposomal celecoxib on proliferation of colon cancer cell and inhibition of DMBA-induced tumor in rat model. Cancer Nanotechnology, 2(1-6), 67-79. https://doi.org/10.1007/s12645-011-0017-5

Provias, J., & Jeynes, B. (2014). Brain pathology brain pathology. Brain Pathology, 24(1), 39-103.

Qayum, A., Rashid, A., Liang, Q., Wu, Y., Cheng, Y., Kang, L., Liu, Y., Zhou, C., Hussain, M., Ren, X., Ashokkumar, M., & Ma, H. (2023). Ultrasonic and homogenization: An overview of the preparation of an edible protein-polysaccharide complex emulsion. Comprehensive Reviews in Food Science and Food Safety, 22(6), 4242-4281. https://doi.org/10.1111/1541-4337.13221

Rice, T., Lachance, D. H., Molinaro, A. M., Eckel-Passow, J. E., Walsh, K. M., Barnholtz-Sloan, J., Ostrom, Q. T., Francis, S. S., Wiemels, J., Jenkins, R. B., Wiencke, J. K., & Wrensch, M. R. (2016). Understanding inherited genetic risk of adult glioma-a review. Neuro-oncology Practice, 3(1), 10-16. https://doi.org/10.1093/nop/npv026

Saad, S., Beg, S., Jain, G. K., & Ahmad, F. J. (2021). Nanostructured therapeutic systems of PUFAs for the treatment of glioblastoma multiforme. Current Drug Metabolism, 22(14), 1087-1102. https://doi.org/10.2174/1389200221666210101115148

Saad, S., Hasan, N., Siddiqui, L., Beg, S., Ali, A., Gupta, A., Jain, G. K., & Ahmad, F. J. (2023). Novel gamma linoleic acid encased in situ lipogel for augmented anti-tumor efficacy against solid tumor: *In vitro* and *in vivo* evaluation. Journal of Drug Delivery Science and Technology, 87, Article 104768. https://doi.org/10.1016/j.jddst.2023.104768

Samyn, P., & Rastogi, V. K. (2022). Stabilization of an aqueous bio-based wax nano-emulsion through encapsulation. Nanomaterials, 12(23), Article 4329. https://doi.org/10.3390/nano12234329

Schaff, L. R., & Mellinghoff, I. K. (2023). Glioblastoma and other primary brain malignancies in adults: A review. JAMA, 329(7), 574-587. https://doi.org/10.1001/jama.2023.0023

Shah, P., Bhalodia, D., & Shelat, P. (2010). Nanoemulsion: A pharmaceutical review. Systematic Reviews in Pharmacy, 1(1), 24. https://doi.org/10.4103/0975-8453.59509

Sheokand, S., Navik, U., & Bansal, A. K. (2019). Nanocrystalline solid dispersions (NSD) of hesperetin (HRN) for prevention of 7, 12-dimethylbenz[a]anthracene (DMBA)-induced breast cancer in Sprague-Dawley (SD) rats. European Journal of Pharmaceutical Sciences, 128, 240-249. https://doi.org/10.1016/j.ejps.2018.12.006

Singh, K., Biharee, A., Vyas, A., Thareja, S., & Jain, A. K. (2022). Recent advancement of polymersomes as drug delivery carrier. Current Pharmaceutical Design, 28(20), 1621-1631. https://doi.org/10.2174/1381612828666220412103552

Smoll, N. R., Brady, Z., Scurrah, K., & Mathews, J. D. (2016). Exposure to ionizing radiation and brain cancer incidence: The Life Span Study cohort. Cancer Epidemiology, 42, 60-65. https://doi.org/10.1016/j.canep.2016.03.006

Sonawane, S. J., Kalhapure, R. S., Jadhav, M., Rambharose, S., Mocktar, C., & Govender, T. (2015). Transforming linoleic acid into a nanoemulsion for enhanced activity against methicillin susceptible and resistant Staphylococcus aureus. RSC Advances, 5(110), 90482-90492. https://doi.org/10.1039/C5RA16248C

Tripathi, C. B., Parashar, P., Arya, M., Singh, M., Kanoujia, J., Kaithwas, G., & Saraf, S. A. (2018). QbD-based development of α-linolenic acid potentiated nanoemulsion for targeted delivery of doxorubicin in DMBA-induced mammary gland carcinoma: *In vitro* and *in vivo* evaluation. Drug Delivery and Translational Research, 8(5), 1313-1334. https://doi.org/10.1007/s13346-018-0525-5

Wang, C., Xu, J., Zhang, Y., & Nie, G. (2023). Emerging nanotechnological approaches to regulating tumor vasculature for cancer therapy. Journal of Controlled Release, 362, 647-666. https://doi.org/10.1016/j.jconrel.2023.09.017

Wang, G., & Wang, W. (2022). Advanced cell therapies for glioblastoma. Frontiers in Immunology, 13, Article 904133. https://doi.org/10.3389/fimmu.2022.904133

Wang, X., Anton, H., Vandamme, T., & Anton, N. (2023). Updated insight into the characterization of nano-emulsions. Expert Opinion on Drug Delivery, 20(1), 93-114. https://doi.org/10.1080/17425247.2023.2154075

Wang, X., Lin, H., & Gu, Y. (2012). Multiple roles of dihomo-γ-linolenic acid against proliferation diseases. Lipids in Health and Disease, 11, 25. https://doi.org/10.1186/1476-511X-11-25

Wooster, T. J., Golding, M., & Sanguansri, P. (2008). Impact of oil type on nanoemulsion formation and Ostwald ripening stability. Langmuir, 24(22), 12758-12765. https://doi.org/10.1021/la801685v

Yaghmour, R., Garajah, M., Kayali, I., & Al-Rimawi, F. (2021). Antioxidant, antimicrobial and formulation of borage (Borago officinalis) seeds oil and leaves extracts as microemulsion. Journal of Pharmaceutical Research International, 33(55A), 136-148. https://doi.org/10.9734/jpri/2021/v33i55A33816

Young, R. M., Jamshidi, A., Davis, G., & Sherman, J. H. (2015). Current trends in the surgical management and treatment of adult glioblastoma. Annals of Translational Medicine, 3(9), Article 121. https://doi.org/10.3978/j.issn.2305-5839.2015.05.10

Zhai, K., Siddiqui, M., Abdellatif, B., Liskova, A., Kubatka, P., & Büsselberg, D. (2021). Natural compounds in glioblastoma therapy: Preclinical insights, mechanistic pathways, and outlook. Cancers, 13(10), Article 2317. https://doi.org/10.3390/cancers13102317

Zuccari, G., & Alfei, S. (2023). Development of phytochemical delivery systems by nano-suspension and nano-emulsion techniques. International Journal of Molecular Sciences, 24(12), Article 9824. https://doi.org/10.3390/ijms24129824

Zwain, T., Alder, J. E., Zwayen, S., Shaw, A., Burrow, A. J., & Singh, K. K. (2023). Overcoming biological barriers BBB/BBTB by designing PUFA functionalised lipid-based nanocarriers for glioblastoma targeted therapy. Biomaterials Advances, 155, Article 213660. https://doi.org/10.1016/j.bioadv.2023.213660

Cite this article: Chaudhari R, Ahmad FJ, Khan K, Ahmad S. Formulation of a Bioactive Nanoemulsion of Gamma Linolenic Acid for Anti-Glioblastoma Activity. Pharmacog Res. 2026;18(2):568-84.

Supplementary File

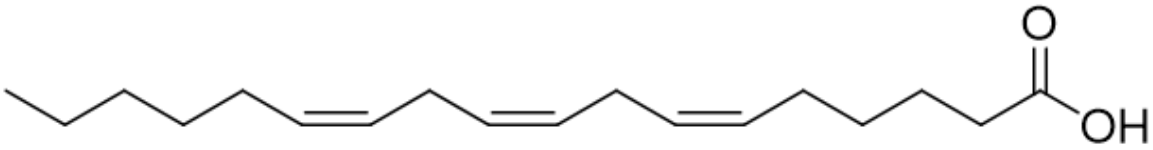

Figure S1: Chemical structure of Gamma-linolenic acid (GLA).

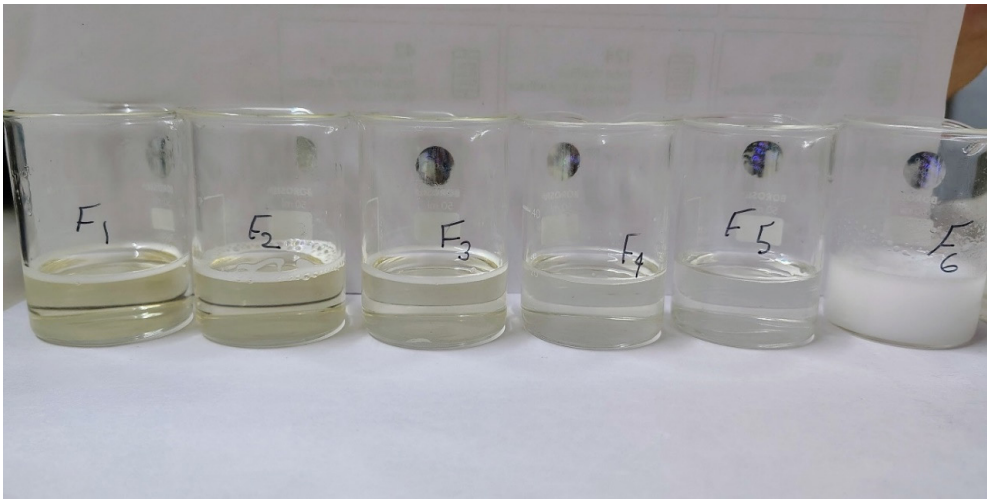

Figure S2: The development of GLA loaded nanoemulsion (GLA-NE).

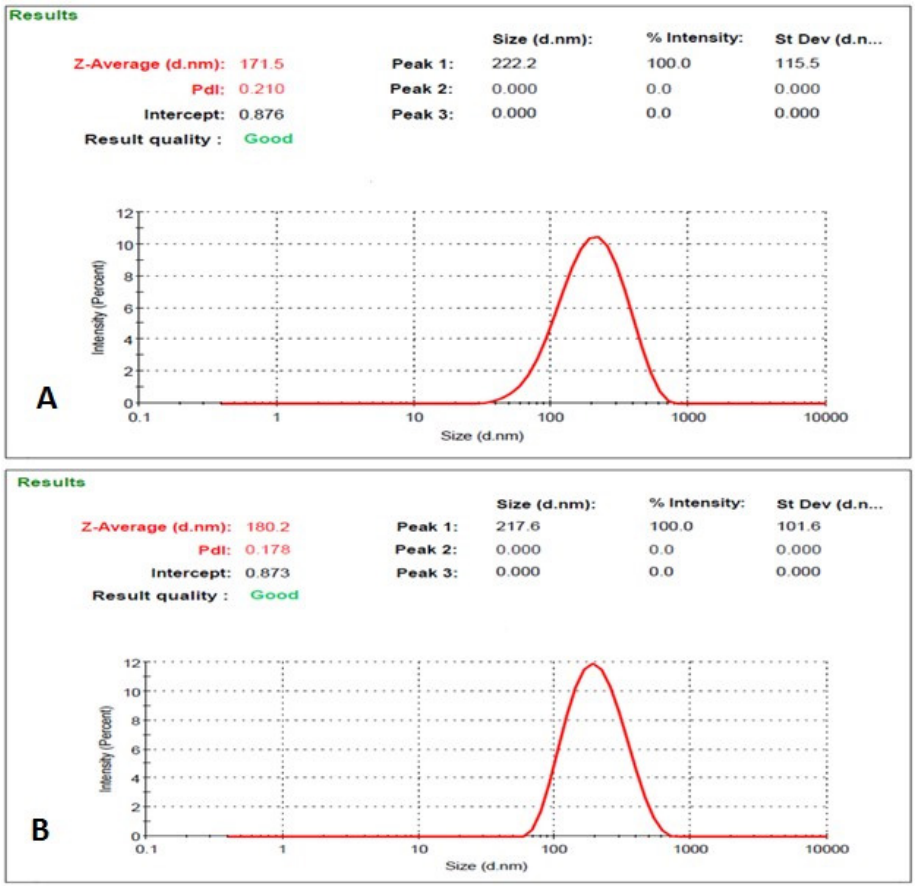

Figure S3: Particle size (nm), PDI of the (a) blank nanoemulsion (171.5± 5.9nm) (b) optimized drug loaded nanoemulsion (180.2± 4.5 nm).

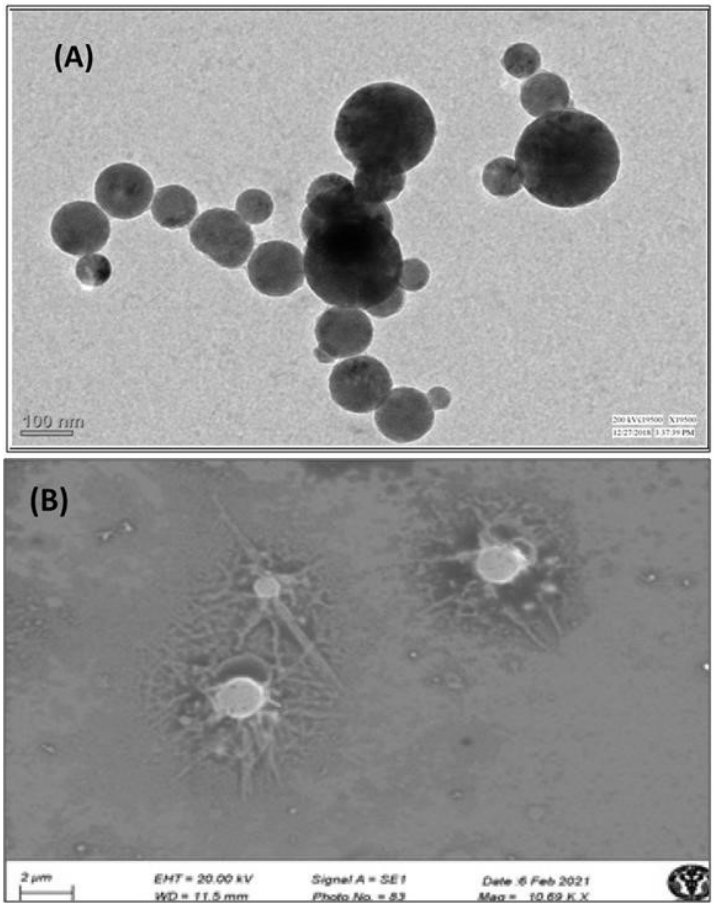

Figure S4: Electron microscopy imaging (a). TEM image of the optimized formulation. (b). SEM image of the optimized formulation.

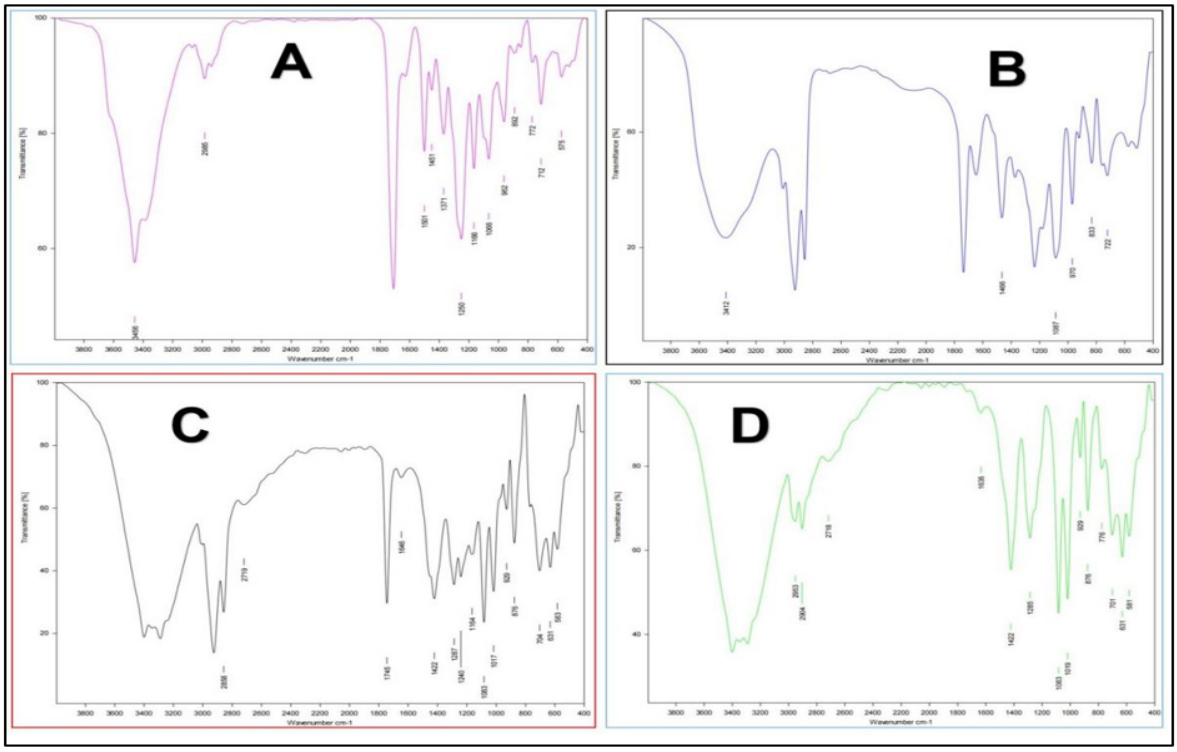

Figure S5: FT-IR spectra of (a) gamma linolenic acid (b) physical mixture of gamma linolenic acid and phospholipid (c) lyophilized nanoformulation (d) pure mannitol.

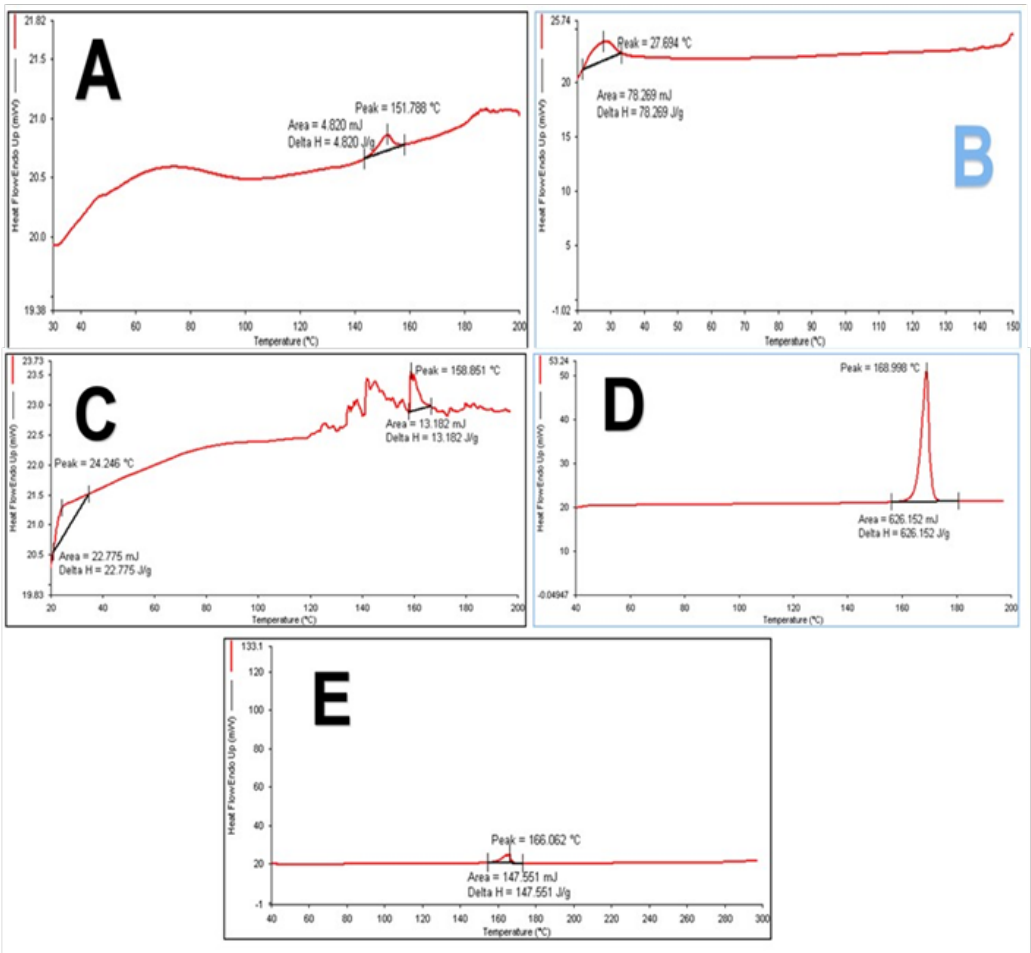

Figure S6: DSC plot of (a) gamma linolenic acid (b) phospholipid (c) physical mixture of doxtaxel and lipid (d) pure mannitol (e) lyopilized formulation.

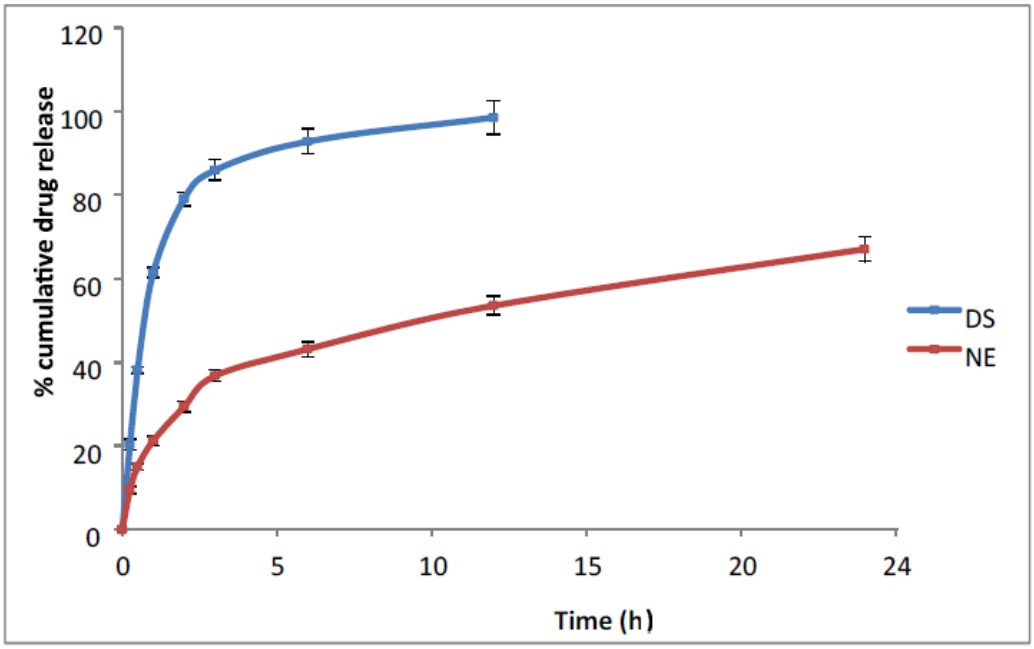

Figure S7: *In vitro* release pattern of the drug (GLA) from the drug suspension and the GLA-nanoemulsion formulation. All values are mentioned as Mean ± SD; n=3.

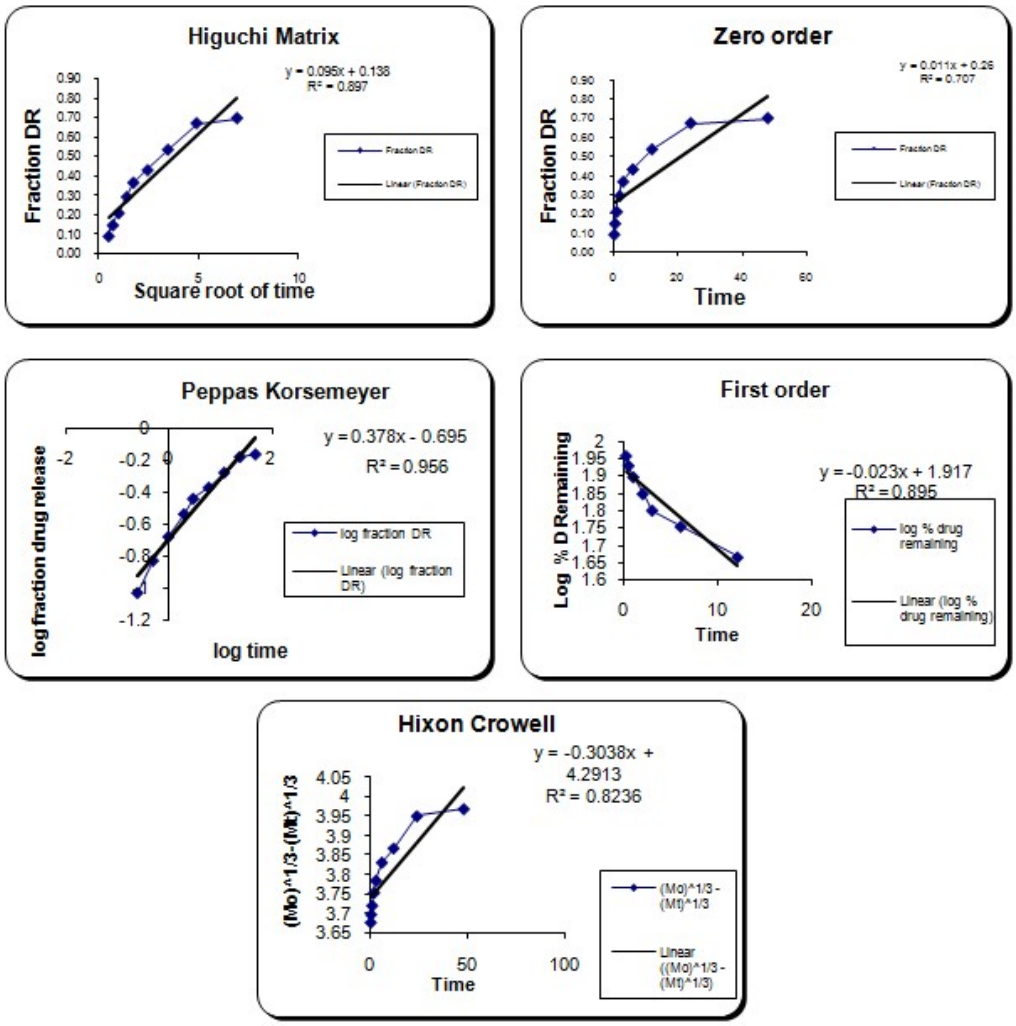

Figure S8: *In vitro* release kinetic models of release of GLA from GLA-NE.

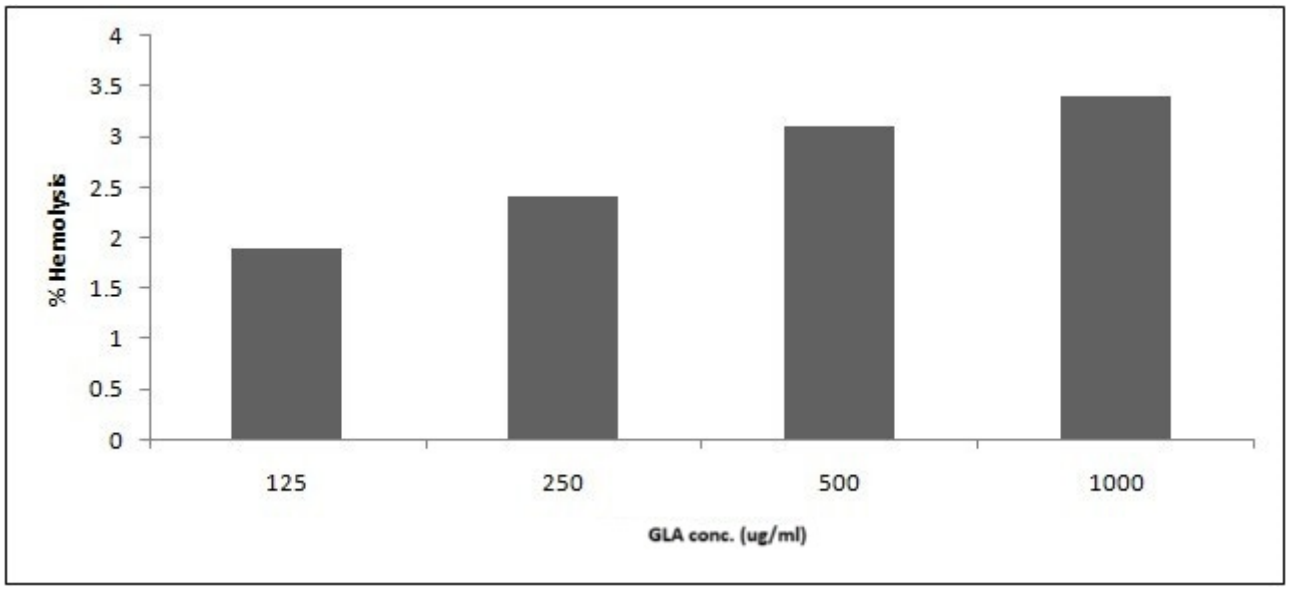

Figure S9: Graph showing the percent (%) hemolysis at different concentration of the nanoemulsion.

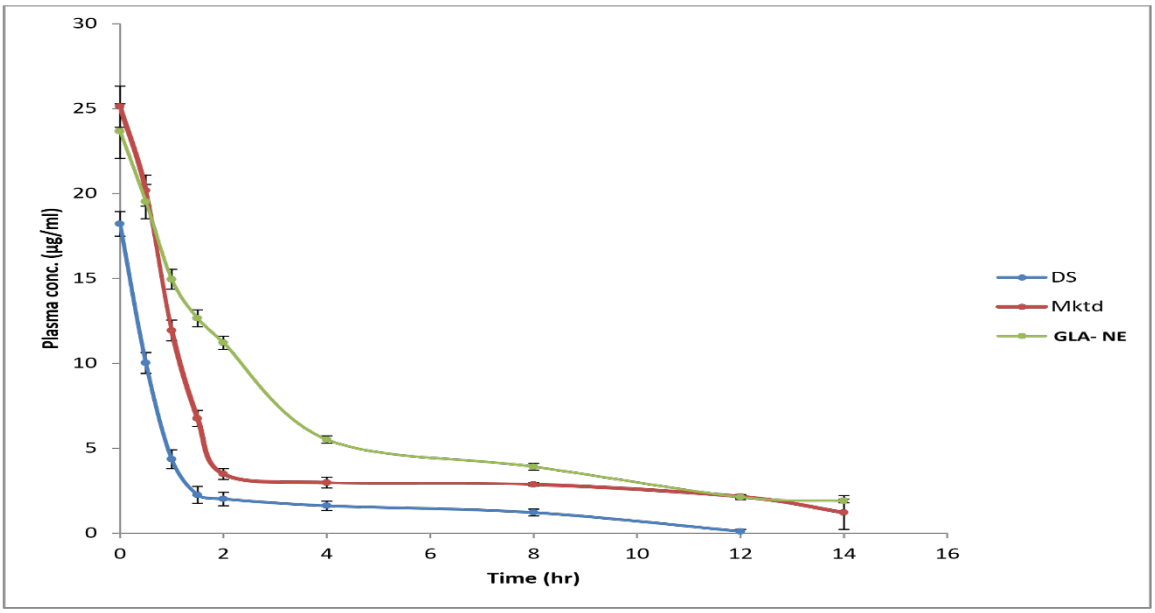

Figure S10: Plasma concentration vs time plot of GLA (pure drug), marteted formulation of GLA and GLA-NE; nanoformulation of GLA after IV.

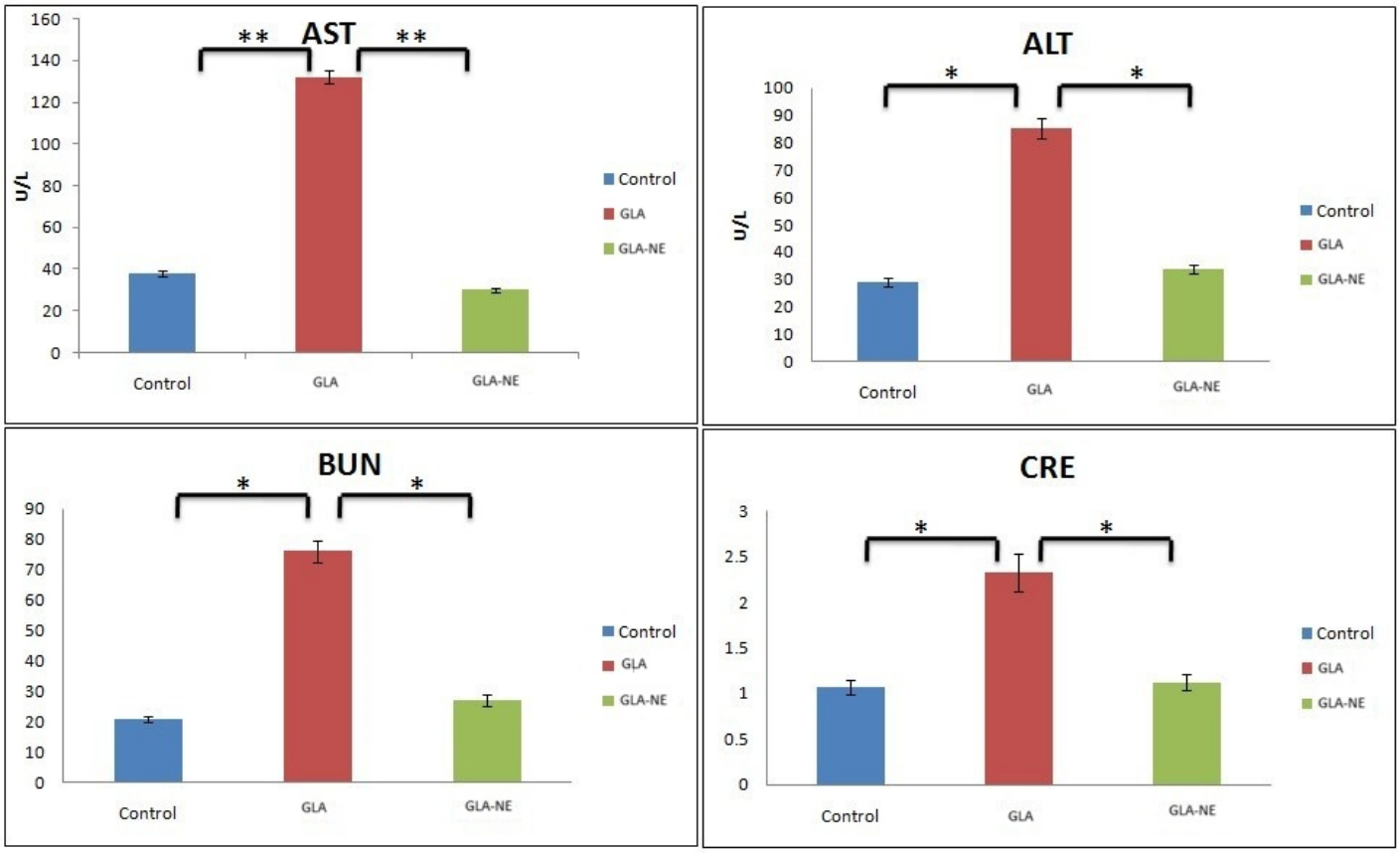

Figure S11: Serum alanine transaminase (ALT), aspartate transaminase (AST), blood urea nitrogen (BUN) after i.v. administration to healthy rats, (* represent $p < 0.05$; ** $p<0.01$).